Figure 3   Two promising compounds of WNK–SPAK-binding inhibitors obtained by FCS screening

(A) Chemical structures and substance names of two promising inhibitors. Compound B1 is a close homologue of compound B that has no inhibitory activity. (B) Confirmation of binding inhibition of WNK4 and SPAK by compounds A and B. The two compounds were added to a mixed solution of TAMRA-WNK4 (RFQV) and GST–SPAK-CCT at various concentrations (1.5–200 μM). The IC$_{50}$ values of compound A and B were 37 μM and 16 μM respectively. Compound B1 showed no inhibitory effect. (C) Confirmation of binding inhibition of WNK1 and SPAK by the compounds. Results similar to (B) were obtained. The IC$_{50}$ values of compound A and B were 30.6 μM and 34.4 μM respectively. Compound B1 showed no inhibitory effect. (D) Binding of the two compounds to the CCT domain of SPAK (GST–SPAK-CCT) determined by Biacore^{TM} assay. Sensorgram shows concentration-dependent binding of two compounds to GST–SPAK-CCT. GST–SPAK-CCT was ligated on to a CM5 sensor chip by standard primary amine coupling chemistry. Compounds were injected for 40 s over the immobilized GST–SPAK-CCT at a flow rate of 60 μl/min. The K_d values (steady state) of compounds A and B were 32 μM and 20 μM respectively. N.D., not determined; RU, response units.

diffusion time was within ± 10 % of the positive control. As a result of the initial screening of 16 902 compounds, we obtained 104 primary hits. Along with the secondary screening, we then checked whether these compounds affected the diffusion time of fluorescent peptide alone to exclude a false-positive effect (Supplementary Figure S2 at http://www.biochemj.org/bj/455/bj4550339add.htm). After checking the false-positive effect and reproducibility (Supplementary Figure S2), 94 compounds were excluded. Finally, ten secondary hits were obtained.

FCS and Biacore^{TM} assays of two promising compounds

Figure 3(A) shows the chemical structure of the two compounds that showed the highest inhibitory activity among the ten secondary hits (compounds A and B) and one close homologue of compound B that has no inhibitory activity (compound B1). The substance names of compounds A and B are STOCK1S-50699 (PubChem-CID 5749625) and STOCK2S-26016 (PubChem-CID 3135086) respectively. Figure 3(B) shows the results of the *in vitro* FCS assay of these drugs for the inhibition of the binding of WNK4 and SPAK. The IC$_{50}$ values of compound A and B were 37 μM and 16 μM respectively. Furthermore, we tested whether the binding of SPAK to WNK1 as well as WNK4 was inhibited by the same compounds. As shown in Figure 3(C), the inhibitory effects of both compounds on WNK1 were similar to those for WNK4. Interestingly, compound B1 (Figure 3A), a structurally

close homologue of compound B, did not show an inhibitory effect in the FCS assay (Figures 3B and 3C), suggesting that the inhibitory effect of compound B might not be a non-specific effect on the binding and also provided some implication about the structure–activity relationship of the inhibitor. In the FCS assay, it is difficult to determine whether the compound binds to WNK or SPAK. Thus, to determine the binding partner, we performed further analysis of the interaction between the hit compounds and GST–SPAK-CCT using Biacore^{TM}. As shown in Figure 3(D), it was confirmed that both compounds bound to GST–SPAK-CCT, although the binding kinetics were different. Compound A showed relatively slow binding and dissociation compared with compound B, which may be a benefit in terms of drug properties. The K_d values (steady state) of compounds A and B obtained by the Biacore^{TM} assay were 32 μM and 20 μM respectively. These values were comparable with the values obtained by the FCS assay, clearly suggesting that both hit compounds inhibited the binding of WNK and SPAK by binding to the CCT domain of SPAK.

The two compounds showed inhibitory effects on hypotonicity-induced WNK-SPAK signalling in mpkDCT and MOVAS cells

Next, we tested whether these compounds possess *in vivo* inhibitory activity for WNK signalling using mpkDCT cells (Figures 4A and 4C), which endogenously express SPAK and
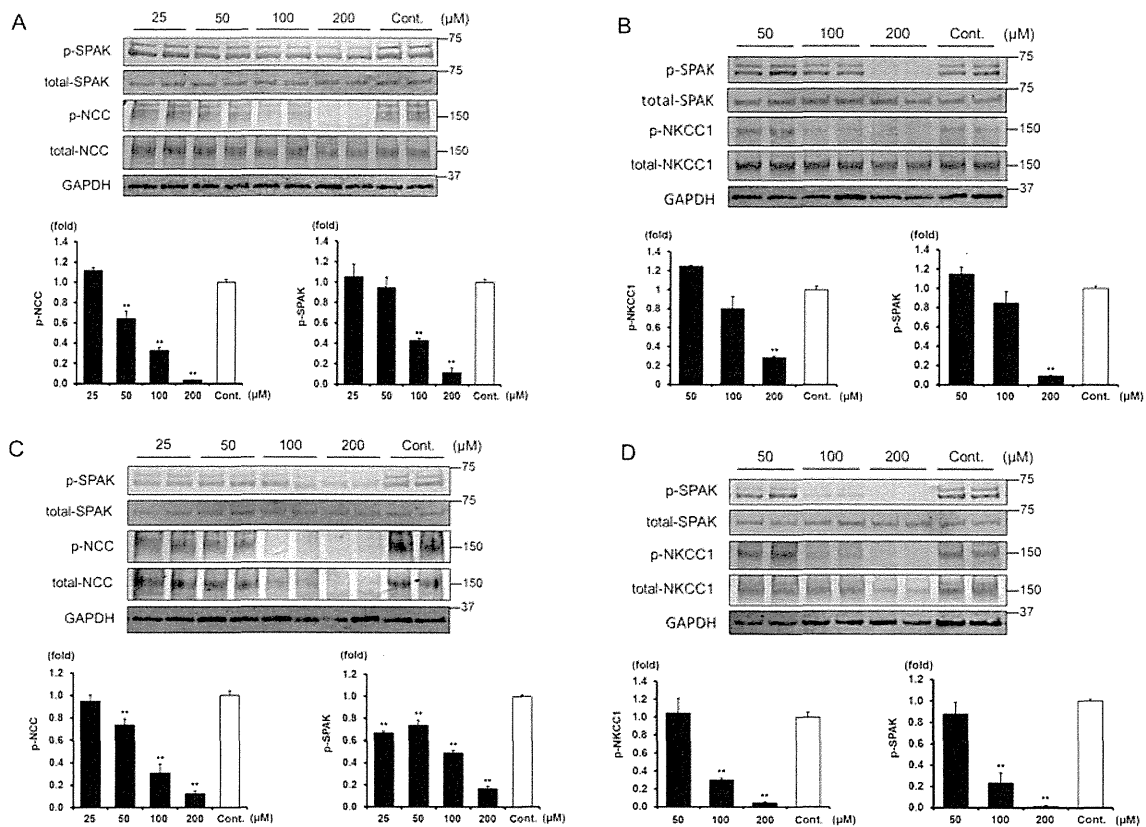
Figure 4   Inhibitory effect of compound A and B on WNK–SPAK signalling in mpkDCT and MOVAS cells

(**A**) The phosphorylation of SPAK and NCC in mpkDCT cells was drastically and dose-dependently reduced by compound A (25–200 μM). The lower panel shows quantification of the results of the blots (**$**P < 0.01, n = 4, means $\pm$ S.E.M.). (**B**) The phosphorylation of SPAK and NKCC1 in MOVAS cells was drastically and dose-dependently reduced by compound A (50–200 μM). The lower panel shows quantification of the results of the blots (**$**P < 0.01, n = 4, means $\pm$ SEM). (**C**) Results similar to (**A**) were obtained by treatment with compound B in mpkDCT cells. (**D**) Results similar to (**B**) were obtained by treatment with compound B in MOVAS cells. Cont., control.

NCC [28], and MOVAS cells (Figures 4B and 4D), which endogenously express SPAK and NKCC1 [31]. We used 45 min of hypotonic shock (170 mOsm/g H_2O) to activate WNK signalling. Both compounds A and B dose-dependently inhibited the phosphorylation of endogenous SPAK and NCC in mpkDCT cells and SPAK and NKCC1 in MOVAS cells. To exclude the possibility that the decreases in phosphorylation were due to non-specific effects of the compounds, we evaluated the effect of these compounds on phospho- and total-p38 MAPK (mitogen-activated protein kinase) expression, which is a separate phosphorylation event from WNK-SPAK signalling. As shown in Supplementary Figure S3 (at http://www.biochemj.org/bj/455/bj4550339add.htm), even with the increased concentrations of the compounds, the phosphorylated p38 expression was not reduced, rather slightly increased by these compounds. Compound B1, a non-inhibitory homologue of compound B, also did not affect the phosphorylation of SPAK and NCC (Supplementary Figure S4 at http://www.biochemj.org/bj/455/bj4550339add.htm). These data serve as negative controls to support the specificity of the inhibitory effect of compounds A and B on WNK-SPAK signalling.

DISCUSSION

The current interest in therapeutic antibodies vividly demonstrates the value of a strategy to create drugs by disrupting protein–

protein interactions [18]. Therapeutic antibodies have some excellent properties: they are highly specific for their molecular targets, and they tend to be stable in human serum. On the other hand, antibodies are difficult and expensive to manufacture, and they lack oral bioavailability. In addition, antibodies are not cell-permeable; therefore, antagonism of intracellular protein–protein systems has been limited so far. In this respect, if the target proteins are cytoplasmic proteins, the development of small compounds that disrupt protein–protein interactions is highly anticipated.

We have developed a novel screening system for binding inhibitors using FCS. As shown in Figure 1, our FCS method succeeded in detecting the binding between WNK and SPAK. Our FCS system has several advantages. First, immobilization of substrates is not required, unlike the Biacore™ system. Secondly, since the assay is performed in aqueous solution, the binding of molecules occurs under more physiological conditions. Thirdly, our system directly assesses the ability of compounds to disrupt the binding of two molecules. Although Biacore™ can detect the binding of compounds to one of the target molecules with high sensitivity, it does not tell us whether the compounds indeed disrupt the binding of two molecules. Furthermore, our system has a great feature capable of high-throughput screening in 384-well plates.

In this FCS system, in order to detect the binding of two molecules the sensitivity would be better when the apparent molecular mass of a fluorophore changes drastically by binding.

Therefore we used TAMRA-labelled WNK peptides as probes. In this respect, their counterpart, SPAK, should be better in the full-length form than in the partial form (GST–SPAK-CCT). However, the full-length GST–SPAK protein was difficult to obtain in a large amount, mainly due to low solubility and recovery. Thus our binding assay was performed with partial proteins of WNK and SPAK. Therefore we might have missed any compounds that have a greater inhibitory effect on the binding of native full-length proteins. This drawback might be a trade-off for the efficiency of our screening system.

As a result of screening for compounds that disrupt the binding of WNK to SPAK, we obtained two compounds that effectively inhibited the signalling from WNK to NCC and NKCC1 in mpkDCT and MOVAS cells respectively. The amount of total NCC/NKCC1 clearly decreased in the presence of these compounds as the phosphorylation decreased. Similar changes were observed in our previous studies [9,32] and in WNK4-knockout mice [14]. Recently, we showed that the NCC phosphorylation regulated its ubiquitination [33], suggesting that the decrease of NCC/NKCC1 phosphorylation would induce the degradation. In this respect, the changes in phosphorylation would be the primary event. Therefore we only presented phosphorylation of NCC/NKCC1 and SPAK data in the histograms of Figure 4. Nonetheless, it is still possible that our compounds might also block the binding of SPAK to NCC/NKCC1, and the complex formation of SPAK and NCC/NKCC1 might somehow be involved in the stability of the transporters. Further investigation may be necessary on this issue.

The results of the present study clearly demonstrate that the binding between WNK and SPAK is indispensable for WNK signalling *in vivo* and that these compounds are the promising seeds of a new class of anti-hypertensive drugs with dual actions of diuresis and vasodilation. In addition to the antihypertensive property of a WNK-SPAK signalling inhibitor, the recent advancement of WNK research has revealed the possibility of additional therapeutic targets of WNK-SPAK inhibition. WNK3 stimulated glioma invasion by regulating cell volume through NKCC1 activation [34,35]. The knockout of SPAK attenuated intestinal inflammation in mice [36,37]. Those studies suggest the possibility of WNK-SPAK signalling inhibitors that are not just anti-hypertensive drugs. Chemical modification of these compounds would give us better compounds that can be used *in vivo*.

In conclusion, we developed a new high-throughput screening system to identify compounds that disrupt the binding of two molecules. By using this method, we found promising seeds of WNK signalling inhibitors.

AUTHOR CONTRIBUTION

Takayasu Mori established the screening system using FCS and performed the chemical library screening, Biacore™ assay and cell culture studies, and wrote the paper. Yuko Watanabe, Mari Ishigami-Yuasa, Shinya Fujii and Hiroyuki Kagechika prepared the compounds in the chemical library. Eriko Kikuchi, Eisei Sohara, Tatemitsu Rai and Sei Sasaki helped Takayasu Mori in general experimental procedures and contributed to data discussion. Shinichi Uchida designed and directed the project and wrote the paper.

FUNDING

REFERENCES

1　Gordon, R. D. (1986) Syndrome of hypertension and hyperkalemia with normal glomerular filtration rate. Hypertension **8**, 93–102

2　Wilson, F. H., Disse-Nicodème, S., Choate, K. A., Ishikawa, K., Nelson-Williams, C., Desitter, I., Gunel, M., Milford, D. V., Lipkin, G. W., Achard, J. M. et al. (2001) Human hypertension caused by mutations in WNK kinases. Science **293**, 1107–1112

3　Kahle, K. T., Rinehart, J., Giebisch, G., Gamba, G., Hebert, S. C. and Lifton, R. P. (2008) A novel protein kinase signaling pathway essential for blood pressure regulation in humans. Trends Endocrinol. Metab. **19**, 91–95

4　McCormick, J. A., Yang, C. L. and Ellison, D. H. (2008) WNK kinases and renal sodium transport in health and disease: an integrated view. Hypertension **51**, 588–596

5　Richardson, C. and Alessi, D. R. (2008) The regulation of salt transport and blood pressure by the WNK-SPAK/OSR1 signalling pathway. J. Cell Sci. **121**, 3293–3304

6　Uchida, S. (2010) Pathophysiological roles of WNK kinases in the kidney. Pflugers Arch. **460**, 695–702

7　Yang, S. S., Morimoto, T., Rai, T., Chiga, M., Sohara, E., Ohno, M., Uchida, K., Lin, S. H., Moriguchi, T., Shibuya, H. et al. (2007) Molecular pathogenesis of pseudohypoaldosteronism type II: generation and analysis of a Wnk4(D561A/+) knockin mouse model. Cell Metab. **5**, 331–344

8　Moriguchi, T., Urushiyama, S., Hisamoto, N., Iemura, S., Uchida, S., Natsume, T., Matsumoto, K. and Shibuya, H. (2005) WNK1 regulates phosphorylation of cation-chloride-coupled cotransporters via the STE20-related kinases, SPAK and OSR1. J. Biol. Chem. **280**, 42685–42693

9　Chiga, M., Rai, T., Yang, S. S., Ohta, A., Takizawa, T., Sasaki, S. and Uchida, S. (2008) Dietary salt regulates the phosphorylation of OSR1/SPAK kinases and the sodium chloride cotransporter through aldosterone. Kidney Int. **74**, 1403–1409

10　Garg, P., Martin, C. F., Elms, S. C., Gordon, F. J., Wall, S. M., Garland, C. J., Sutliff, R. L. and O'Neill, W. C. (2007) Effect of the Na-K-2Cl cotransporter NKCC1 on systemic blood pressure and smooth muscle tone. Am. J. Physiol. Heart Circ. Physiol. **292**, H2100–H2105

11　Akar, F., Jiang, G., Paul, R. J. and O'Neill, W. C. (2001) Contractile regulation of the Na$^+$-K$^+$-2Cl$^-$ cotransporter in vascular smooth muscle. Am. J. Physiol. Cell Physiol. **281**, C579–C584

12　Meyer, J. W., Flagella, M., Sutliff, R. L., Lorenz, J. N., Nieman, M. L., Weber, C. S., Paul, R. J. and Shull, G. E. (2002) Decreased blood pressure and vascular smooth muscle tone in mice lacking basolateral Na$^+$-K$^+$-2Cl$^-$ cotransporter. Am. J. Physiol. Heart Circ. Physiol. **283**, H1846–H1855

13　Talati, G., Ohta, A., Rai, T., Sohara, E., Naito, S., Vandewalle, A., Sasaki, S. and Uchida, S. (2010) Effect of angiotensin II on the WNK-OSR1/SPAK-NCC phosphorylation cascade in cultured mpkDCT cells and in vivo mouse kidney. Biochem. Biophys. Res. Commun. **393**, 844–848

14　Castañeda-Bueno, M., Cervantes-Pérez, L. G., Vázquez, N., Uribe, N., Kantesaria, S., Morla, L., Bobadilla, N. A., Doucet, A., Alessi, D. R. and Gamba, G. (2012) Activation of the renal Na$^+$:Cl$^-$ cotransporter by angiotensin II is a WNK4-dependent process. Proc. Natl. Acad. Sci. U.S.A. **109**, 7929–7934

15　Sohara, E., Rai, T., Yang, S. S., Ohta, A., Naito, S., Chiga, M., Nomura, N., Lin, S. H., Vandewalle, A., Ohta, E. et al. (2011) Acute insulin stimulation induces phosphorylation of the Na-Cl cotransporter in cultured distal mpkDCT cells and mouse kidney. PLoS ONE **6**, e24277

16　Nishida, H., Sohara, E., Nomura, N., Chiga, M., Alessi, D. R., Rai, T., Sasaki, S. and Uchida, S. (2012) Phosphatidylinositol 3-kinase/Akt signaling pathway activates the WNK-OSR1/SPAK-NCC phosphorylation cascade in hyperinsulinemic db/db mice. Hypertension **60**, 981–990

17　Chen, J., Gu, D., Huang, J., Rao, D. C., Jaquish, C. E., Hixson, J. E., Chen, C. S., Lu, F., Hu, D., Rice, T. et al. (2009) Metabolic syndrome and salt sensitivity of blood pressure in non-diabetic people in China: a dietary intervention study. Lancet **373**, 829–835

18　Arkin, M. R. and Wells, J. A. (2004) Small-molecule inhibitors of protein-protein interactions: progressing towards the dream. Nat. Rev. Drug Discov. **3**, 301–317

19　Hu, L., Magesh, S., Chen, L., Wang, L., Lewis, T. A., Chen, Y., Khodier, C., Inoyama, D., Beamer, L. J., Emge, T. J. et al. (2013) Discovery of a small-molecule inhibitor and cellular probe of Keap1-Nrf2 protein-protein interaction. Bioorg. Med. Chem. Lett. **23**, 3039–3043

20　Clark, R. C., Lee, S. Y., Searcey, M. and Boger, D. L. (2009) The isolation, total synthesis and structure elucidation of chlorofusin, a natural product inhibitor of the p53-mDM2 protein-protein interaction. Nat. Prod. Rep. **26**, 465–477

21　Berg, T. (2008) Small-molecule inhibitors of protein-protein interactions. Curr. Opin. Drug Discov. Devel. **11**, 666–674

22　Vitari, A. C., Thastrup, J., Rafiqi, F. H., Deak, M., Morrice, N. A., Karlsson, H. K. and Alessi, D. R. (2006) Functional interactions of the SPAK/OSR1 kinases with their upstream activator WNK1 and downstream substrate NKCC1. Biochem. J. **397**, 223–231

23 Diepens, R. J., den Dekker, E., Bens, M., Weidema, A. F., Vandewalle, A., Bindels, R. J. and Hoenderop, J. G. (2004) Characterization of a murine renal distal convoluted tubule cell line for the study of transcellular calcium transport. Am. J. Physiol. Renal Physiol. **286**, F483–F489

24 Naito, S., Ohta, A., Sohara, E., Ohta, E., Rai, T., Sasaki, S. and Uchida, S. (2011) Regulation of WNK1 kinase by extracellular potassium. Clin. Exp. Nephrol. **15**, 195–202

25 Ohno, M., Uchida, K., Ohashi, T., Nitta, K., Ohta, A., Chiga, M., Sasaki, S. and Uchida, S. (2011) Immunolocalization of WNK4 in mouse kidney. Histochem. Cell Biol. **136**, 25–35

26 Yang, S. S., Lo, Y. F., Wu, C. C., Lin, S. W., Yeh, C. J., Chu, P., Sytwu, H. K., Uchida, S., Sasaki, S. and Lin, S. H. (2010) SPAK-knockout mice manifest Gitelman syndrome and impaired vasoconstriction. J. Am. Soc. Nephrol. **21**, 1868–1877

27 Kuroki, K., Kobayashi, S., Shiroishi, M., Kajikawa, M., Okamoto, N., Kohda, D. and Maenaka, K. (2007) Detection of weak ligand interactions of leukocyte Ig-like receptor B1 by fluorescence correlation spectroscopy. J. Immunol. Methods **320**, 172–176

28 Richardson, C., Rafiqi, F. H., Karlsson, H. K., Moleleki, N., Vandewalle, A., Campbell, D. G., Morrice, N. A. and Alessi, D. R. (2008) Activation of the thiazide-sensitive Na$^+$-Cl$^-$ cotransporter by the WNK-regulated kinases SPAK and OSR1. J. Cell Sci. **121**, 675–684

29 Pacheco-Alvarez, D., Vázquez, N., Castañeda-Bueno, M., de-Los-Heros, P., Cortes-González, C., Moreno, E., Meade, P., Bobadilla, N. A. and Gamba, G. (2012) WNK3-SPAK interaction is required for the modulation of NCC and other members of the SLC12 family. Cell. Physiol. Biochem. **29**, 291–302

30 Ohta, A., Rai, T., Yui, N., Chiga, M., Yang, S. S., Lin, S. H., Sohara, E., Sasaki, S. and Uchida, S. (2009) Targeted disruption of the Wnk4 gene decreases phosphorylation of Na-Cl cotransporter, increases Na excretion and lowers blood pressure. Hum. Mol. Genet. **18**, 3978–3986

31 Koltsova, S. V., Kotelevtsev, S. V., Tremblay, J., Hamet, P. and Orlov, S. N. (2009) Excitation-contraction coupling in resistance mesenteric arteries: evidence for NKCC1-mediated pathway. Biochem. Biophys. Res. Commun. **379**, 1080–1083

32 Chiga, M., Rafiqi, F. H., Alessi, D. R., Sohara, E., Ohta, A., Rai, T., Sasaki, S. and Uchida, S. (2011) Phenotypes of pseudohypoaldosteronism type II caused by the WNK4 D561A missense mutation are dependent on the WNK-OSR1/SPAK kinase cascade. J. Cell Sci. **124**, 1391–1395

33 Hossain Khan, M. Z., Sohara, E., Ohta, A., Chiga, M., Inoue, Y., Isobe, K., Wakabayashi, M., Oi, K., Rai, T., Sasaki, S. and Uchida, S. (2012) Phosphorylation of Na-Cl cotransporter by OSR1 and SPAK kinases regulates its ubiquitination. Biochem. Biophys. Res. Commun. **425**, 456–461

34 Garzon-Muvdi, T., Schiapparelli, P., ap Rhys, C., Guerrero-Cazares, H., Smith, C., Kim, D. H., Kone, L., Farber, H., Lee, D. Y., An, S. S., Levchenko, A. and Quiñones-Hinojosa, A. (2012) Regulation of brain tumor dispersal by NKCC1 through a novel role in focal adhesion regulation. PLoS Biol. **10**, e1001320

35 Haas, B. R., Cuddapah, V. A., Watkins, S., Rohn, K. J., Dy, T. E. and Sontheimer, H. (2011) With-no-lysine kinase 3 (WNK3) stimulates glioma invasion by regulating cell volume. Am. J. Physiol. Cell Physiol. **301**, C1150–C1160

36 Yan, Y., Laroui, H., Ingersoll, S. A., Ayyadurai, S., Charania, M., Yang, S., Dalmasso, G., Obertone, T. S., Nguyen, H., Sitaraman, S. V. and Merlin, D. (2011) Overexpression of Ste20-related proline/alanine-rich kinase exacerbates experimental colitis in mice. J. Immunol. **187**, 1496–1505

37 Zhang, Y., Viennois, E., Xiao, B., Baker, M. T., Yang, S., Okoro, I. and Yan, Y. (2013) Knockout of Ste20-like proline/alanine-rich kinase (SPAK) attenuates intestinal inflammation in mice. Am. J. Pathol. **182**, 1617–1628

SUPPLEMENTARY ONLINE DATA
Chemical library screening for WNK signalling inhibitors using fluorescence correlation spectroscopy

Takayasu MORI*, Eriko KIKUCHI*, Yuko WATANABE†, Shinya FUJII†, Mari ISHIGAMI-YUASA‡, Hiroyuki KAGECHIKA†‡, Eisei SOHARA*, Tatemitsu RAI*, Sei SASAKI* and Shinichi UCHIDA*[1]

*Department of Nephrology, Graduate School of Medical and Dental Sciences, Tokyo Medical and Dental University, 1-5-45 Yushima, Bunkyo, Tokyo 113-8519, Japan, †Institute of Biomaterials and Bioengineering, Tokyo Medical and Dental University, 1-5-45 Yushima, Bunkyo, Tokyo 113-8519, Japan, and ‡Chemical Biology Screening Center, Tokyo Medical and Dental University, 1-5-45 Yushima, Bunkyo, Tokyo, 113-8519, Japan
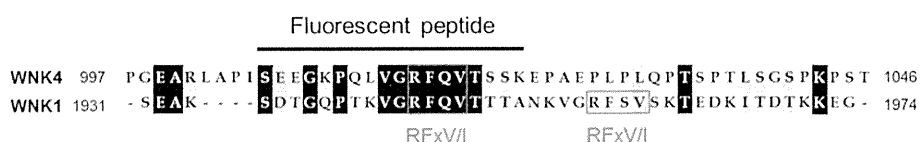
Figure S1   Alignments of WNK4 and WNK1 sequences around RFxV/I motif and TAMRA-labelled WNK4 and WNK1 peptides used for FCS assay

Identical residues are highlighted in black and similar residues are in grey.

---

[1] To whom correspondence should be addressed (email suchida.kid@tmd.ac.jp).

(Fold)

Primary hit compounds (No.)

(Fold)

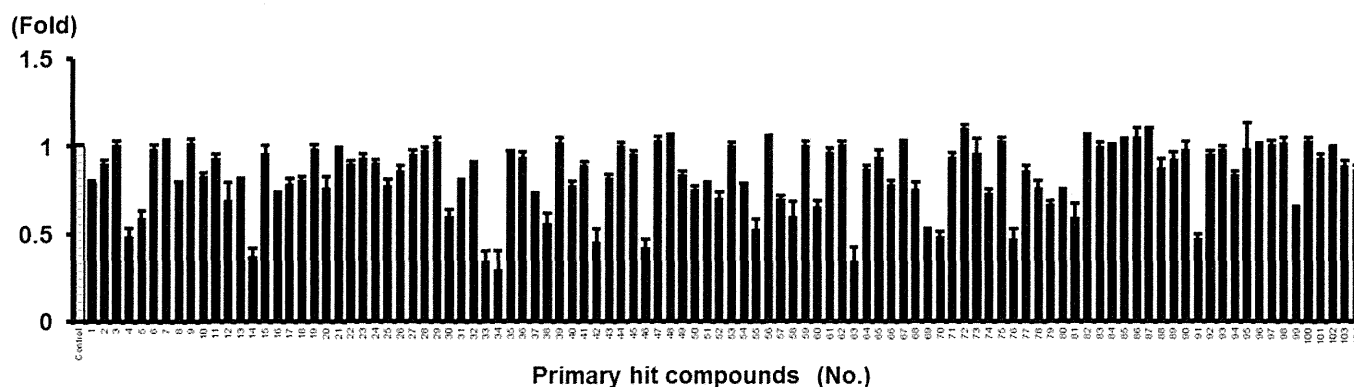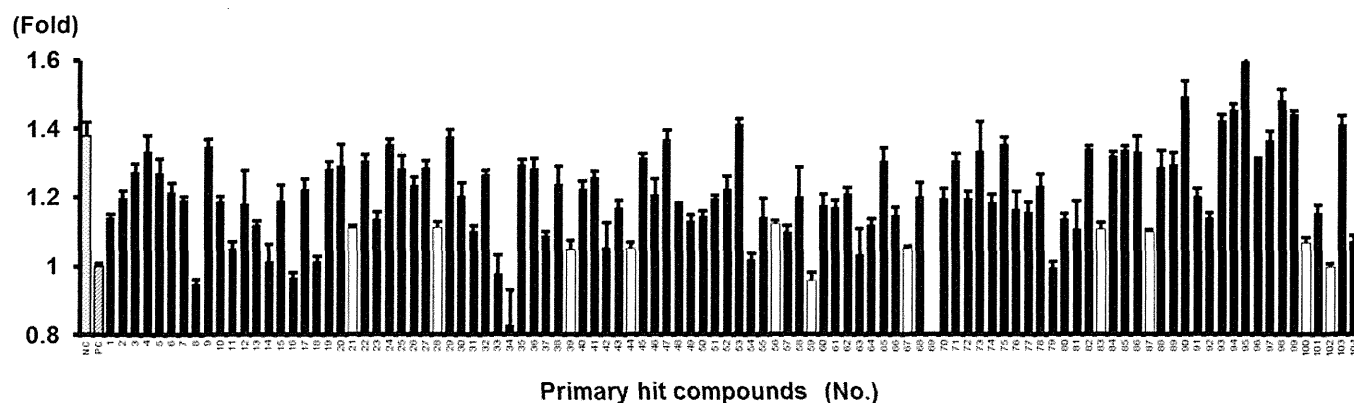Primary hit compounds (No.)

Figure S2   Confirmation of the primary hit compounds

The upper panel shows the secondary screening of the primary hit compounds. The assay was performed under the same conditions as the initial screening (the concentrations of screening compounds were 100 μM). The lower panel shows the effects of the primary hit compounds on the diffusion time of TAMRA-labelled WNK4 peptide without GST–SPAK-CCT. The compounds shown as white bars in upper panel were effective in the restoration of the diffusion time, which was not due to the direct effect on the WNK4 peptide (lower panel). NC, negative control; No., number; PC, positive control.
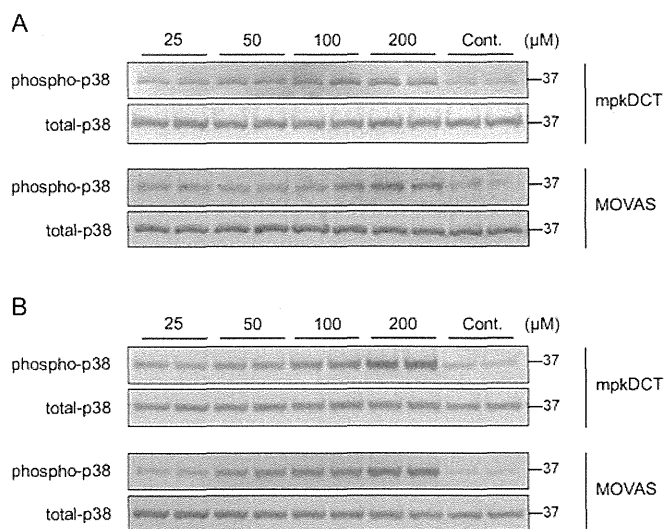

A

Figure S4   Inhibitory effect of compound B1 on WNK-SPAK signalling in mpkDCT cells

The phosphorylation of SPAK and NCC in mpkDCT cells were not affected by compound B1 (25–200 μM).

B

Figure S3   Effect of compounds A and B on p38 MAPK in mpkDCT and MOVAS cells

(A) Phospho-p38 MAPK and total p38 MAPK endogenously expressed in mpkDCT and MOVAS cells were not reduced by compound A (25–200 μM). (B) Results similar to (A) were obtained by the treatment with compound B in mpkDCT and MOVAS cells.
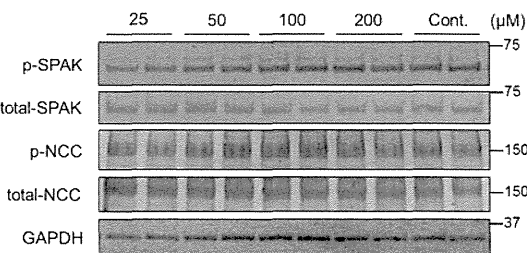
Decrease of WNK4 ubiquitination by disease-causing mutations of KLHL3 through different molecular mechanisms

CrossMark

Yutaro Mori, Mai Wakabayashi, Takayasu Mori, Yuya Araki, Eisei Sohara, Tatemitsu Rai, Sei Sasaki, Shinichi Uchida [*]

Department of Nephrology, Graduate School of Medical and Dental Sciences, Tokyo Medical and Dental University, 1-5-45 Yushima, Bunkyo, Tokyo 113-8519, Japan

A R T I C L E   I N F O

A B S T R A C T

Recently, we demonstrated that WNK4 is a substrate for KLHL3–Cullin3 (CUL3) E3 ubiquitin ligase complexes and that impaired WNK4 ubiquitination is a common mechanism for pseudohypoaldosteronism type II (PHAII) caused by WNK4, KLHL3, and CUL3 mutations. Among the various KLHL3 mutations that cause PHAII, we demonstrated that the R528H mutation in the Kelch domain decreased the binding to WNK4, thereby causing less ubiquitination and increased intracellular levels of WNK4. However, the pathogenic mechanisms of PHAII caused by other KLHL3 mutants remain to be determined. In this study, we examined the pathogenic effects of three PHAII-causing mutations in different KLHL3 domains; the protein levels of these mutants significantly differed when they were transiently expressed in HEK293T cells. In particular, S410L expression was low even with increased plasmid expression. The cycloheximide chase assay revealed that an S410L mutation in the Kelch domain significantly decreased the intracellular stability. Mutations in E85A in the BTB domain and C164F in the BACK domain decreased the binding to CUL3, and S410L as well as R528H demonstrated less binding to WNK4. In vitro and in vivo assays revealed that these mutants decreased the ubiquitination and increased the intracellular levels of WNK4 compared with wild-type KLHL3. Therefore, the KLHL3 mutants causing PHAII investigated in this study exhibited less ability to ubiquitinate WNK4 because of KLHL3's low stability and/or decreased binding to CUL3 or WNK4.

© 2013 Elsevier Inc. All rights reserved.

1. Introduction

Pseudohypoaldosteronism type II (PHAII) is a hereditary disease characterized by hypertension, hyperkalemia, and metabolic acidosis [1]. Mutations in the with-no-lysine kinase 1 (WNK1) and WNK4 genes are known to be responsible for PHAII [2]. Several in vitro and in vivo studies have been performed to clarify the molecular pathogenesis of PHAII [3,4]. We discovered a novel phosphorylation signal cascade in the kidney that consisted of WNK-oxidative stress-responsive kinase 1 (OSR1) and STE20/SPS1-related proline/alkaline-rich kinase (SPAK)–NaCl cotransporter (NCC) [5–8]. The constitutive activation of this cascade is the pathogenic molecular mechanism for PHAII caused by WNK4.

In 2012, two new genes KLHL3 and Cullin3 (CUL3) were reported as being responsible for PHAII [9,10]. KLHL3 is a member of the BTB–BACK–Kelch family of proteins, some of which were reported to function as substrate adapters in CUL3-based E3 ubiquitin ligase complexes [11–13]. We have previously reported that WNK4 is a target for ubiquitination by the KLHL3–CUL3 E3 ligase

complex [14] and that the PHAII-causing mutations of WNK4 and KLHL3 (i.e., D564A and R528H, respectively) impaired the binding of WNK4 and KLHL3, thereby reducing WNK4 ubiquitination and increasing the intracellular protein levels of WNK4. Although the role of WNK4 in NCC regulation is controversial, our recent study using WNK4 transgenic mice clearly indicated that increased WNK4 expression activated the WNK–OSR1/SPAK–NCC cascade and caused PHAII [14]. Taken together, these findings indicated that PHAII was caused by impaired ubiquitination of WNK4. Two recent reports have supported this conclusion [15,16]. Furthermore, it has been reported that the KLHL3–CUL3 E3 ligase complex ubiquitinates WNK1 in vitro [17], and very recently, we demonstrated that KLHL2, which possesses 84% amino acid identity with KLHL3 in the Kelch domain, also acts with CUL3 as an E3 ubiquitin ligase for WNK kinases [18]. Therefore, various combinations of KLHL2 and KLHL3 with the four types of WNK kinases (WNK1–4) may regulate the WNK signal cascades in different types of cells.

Because the above concept is based on the analysis of a single mutant of KLHL3 and WNK4 that causes PHAII [14], we conducted the current study to examine the pathogenic effects of other mutants of KLHL3 and further establish the molecular pathogenesis of PHAII. KLHL3 is composed of the BTB, BACK, and Kelch domains. The R528H mutation, which we previously characterized, is located

* Corresponding author. Fax: +81 3 5803 5215.
   E-mail address: suchida.kid@tmd.ac.jp (S. Uchida).

in the Kelch domain. Consistent with its role of substrate binding in the Kelch domains, R528H revealed less binding to WNK4, thereby causing less ubiquitination and increased intracellular protein levels of WNK4 [14]. Therefore, we selected other mutants from different domains in this study (Fig. 1), namely E85A (BTB domain) and C164F (BACK domain). Moreover, we focused on another mutant in the Kelch domain, S410L, because it may have a novel pathogenic effect that is not observed with R528H.

2. Materials and methods

2.1. Plasmids

Expression plasmids for 3×FLAG-tagged human WNK4 have been previously described [19]. The cDNA encoding Halo-tagged human wild-type (WT)-KLHL3 (Halo-WT-KLHL3) in the pFN21A vector was purchased from Promega. The disease-causing mutations (E85A, C164F, S410L, and R528H) were introduced using a QuickChange Site-directed Mutagenesis Kit (Stratagene). Human CUL3 cDNA was isolated using the reverse transcription–polymerase chain reaction (RT-PCR) using human prostate mRNA as a template and then cloned into the 3×FLAG-CMV10 vector (Sigma–Aldrich). The HA$_4$-tagged ubiquitin expression vector was kindly provided by T. Ohta (School of Medicine, St. Marianna University).

2.2. Cell culture and transfections

HEK293T cells were cultured at 37 °C in a humidified 5% CO$_2$ atmosphere in Dulbecco's modified Eagle's medium (DMEM) supplemented with 10% (v/v) fetal bovine serum (FBS), 2 mM L-glutamine, 100 U/ml penicillin, and 0.1 mg/ml streptomycin. HEK293T cells (3 × 10^5 cells/6-cm dish or 1 × 10^5 cells/3.5-cm dish) were transfected with the indicated amount of plasmid DNA using the Lipofectamine 2000 reagent (Invitrogen).

2.3. Immunoprecipitation

HEK293T cells transfected with the indicated amount of DNA were lysed in a buffer [50 mM Tris–HCl (pH 7.5), 150 mM NaCl, 1% Nonidet P-40, 1 mM sodium orthovanadate, 50 mM sodium fluoride, and protease inhibitor cocktail] for 30 min at 4 °C. For proteasome inhibition, HEK293T cells were treated with 1 μM epoxomicin (Peptide Institute, Osaka, Japan) for 3 h before harvesting. After centrifugation at 12,000×g for 15 min, the protein concentration of the supernatants was measured, and equal amounts were used for immunoprecipitation with anti-FLAG M2 beads (Sigma–Aldrich) or anti-Halo beads (Promega) for 2 h at 4 °C. Thereafter, the immunoprecipitates were washed with the lysis buffer and eluted in SDS sample buffer after boiling for 5 min. To detect WNK4 ubiquitination in the denatured samples, the cells transfected with various plasmids were lysed in 2% SDS buffer [2% SDS, 150 mM NaCl, 10 mM Tris–HCl (pH 8.0), 2 mM sodium orthovanadate, 50 mM sodium fluoride, and 1× protease

inhibitor cocktail] and then boiled for 10 min, followed by sonication. Before immunoprecipitation, the lysates were diluted at 1:10 in a dilution buffer [10 mM Tris–HCl (pH 8.0), 150 mM NaCl, 2 mM EDTA, and 1% Triton X-100], incubated at 4 °C for 1 h with rotation, and centrifuged at 12,000×g for 15 min.

2.4. Antibodies

The blots were probed using the following primary antibodies: anti-FLAG (Sigma–Aldrich), anti-Halo (Promega), anti-HA (Merck Millipore), and anti-GAPDH (Cell Signaling Technology). Alkaline phosphatase-conjugated anti-IgG antibodies (Promega) were used as the secondary antibodies for immunoblotting, and the signals were detected by the Western blue Stabilized Substrate for Alkaline Phosphatase (Promega).

2.5. Cycloheximide chase assay

HEK293T cells (6 × 10^5 cells in 6-well plates) were transfected using the Lipofectamine 2000 reagent with 1 μg of Halo-WT-KLHL3, or 4 μg of either Halo-S410L or R528H–KLHL3. The cells were then cultured for 24 h, followed by incubation with 100 μM cycloheximide. After incubation for the indicated time periods, the cells were washed with PBS and suspended in 50-μl lysis buffer. Thereafter, the cleared lysate (10 μl) was subjected to immunoblot analyses with anti-Halo (Promega).

2.6. Fluorescence correlation spectroscopy (FCS)

Fluorescent TAMRA-labeled WNK4 peptides covering the PHAII mutation sites were prepared (Hokkaido System Science Co., Ltd., Hokkaido, Japan). The sequences of these peptides have been previously reported [14]. Human full-length KLHL3 (wild-type and mutants) was cloned into pGEX6P-1 vectors. The recombinant GST-fusion KLHL3 protein expressed in the BL21 Escherichia coli cells was purified using glutathione Sepharose beads. The TAMRA-labeled WNK4 peptides were incubated at room temperature for 30 min with different concentrations of GST-KLHL3s (0–2 μM) in 1× PBS containing 0.05% Tween 20 (reaction buffer). Further, FCS was performed to measure single-molecule fluorescence using the FluoroPoint-light analytical system (Olympus, Tokyo, Japan) [14,18,20]. The assays were performed in 384-well plates, with all the experiments including 10s of data acquisition. The measurements were repeated five times per sample.

2.7. In vitro ubiquitination assay

cDNA encoding human WNK4 (490–626) with a C-terminal His-tag was amplified by PCR and cloned into a pGEX6p-1 vector. Recombinant GST-fusion WNK4 protein expressed in BL21 E. coli cells was purified using glutathione Sepharose beads. KLHL3–CUL3 complexes were immunoprecipitated from the lysates of HEK293T cells transiently expressing Halo-KLHL3. We have previously reported that CUL3 overexpression is not necessary for the in vitro ubiquitination assay, because HEL293T cells contain abundant endogenous CUL3 [18]. Thereafter, the complexes were incubated in a 20-μl reaction buffer [50 mM Tris–HCl (pH 7.4), 2.5 mM MgCl$_2$, 0.5 mM DTT, 2 mM ATP] for 2 h at 30 °C with purified GST-WNK4-His (1 μg), 100 ng recombinant human E1 (Boston Biochem.), 500 ng recombinant human UbcH5a/UBE2D1 (Boston Biochem.), and 2.5 μg recombinant HA-tagged human ubiquitin (Boston Biochem.). The reaction was terminated by addition of SDS–PAGE sample buffer, followed by boiling for 5 min. The reaction mixtures were then subjected to immunoblot analyses with anti-Ub (Cell Signaling Technology) or His (Abcam) antibodies.
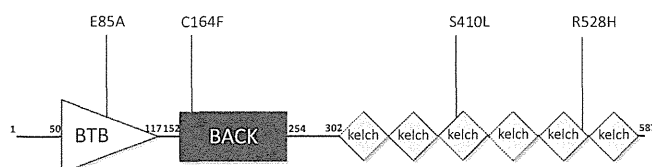

Fig. 1. Structure of human KLHL3 and PHAII mutations analyzed in this study. KLHL3 is composed of BTB, BACK, and Kelch repeat domains. We selected four PHAII-causing KLHL3 mutants for the purpose of evaluation in this study.

2.8. Statistical analysis

Comparisons between the two groups were performed using the unpaired *t*-tests. Analysis of variance with the Tukey's post hoc test was used to evaluate the statistical significance of the comparisons between multiple groups. *P* values <0.05 were considered statistically significant. Data are presented as the mean ± S.E.M.

3. Results and discussion

3.1. Low expression levels of S410L and R528H in HEK293T cells

To analyze each mutant causing PHAII (Fig. 1), we transiently expressed the Halo-tagged KLHL3 (wild-type and mutant) in HEK293T cells. We observed that the expression levels of S410L and R528H appeared to be lower compared with those in the wild-type (WT) and other mutants (Fig. 2A). To confirm this finding, we compared the expression levels of the wild-type and the abovementioned two mutants using different amounts of expression plasmids. As presented in Fig. 2B, the expression levels of these mutants, particularly S410L, was considerably lower compared with that in the wild-type. Because all the KLHL3 expression vectors were the same, we suspected that the missense mutants may have degraded more rapidly in the cells, probably by an endoplasmic reticulum quality control system.

3.2. Significantly decreased stability of S410L

To evaluate the mechanism responsible for the low expression levels of S410L and R528H, we measured the stability of these mutants using the cycloheximide chase assay. As presented in Fig. 2C, S410L was degraded more rapidly than WT–KLHL3. The half-life of S410L was about 6 h, whereas the protein levels of WT–KLHL3 were stable for at least 12 h after cycloheximide treatment.

Contrary to our expectations, the stability of R528H was not decreased compared with that of WT–KLHL3. These results suggest that the pathogenic effects of the S410L mutation may be attributable to the decreased intracellular expression levels resulting from decreased stability. It is possible that the low R528H expression may be attributable to its low translation efficiency, although this remains to be established.

3.3. Impaired binding of the mutant KLHL3 to WNK4 or CUL3

Using immunoprecipitation, we previously demonstrated that the R528H mutation in the Kelch domain decreased its binding to the acidic domain of WNK4 [14]. The current study involved direct measurements of the binding ability of various KLHL3 mutants, including R528H, to WNK4. These measurements were performed using our recently developed FCS method [14,18]. We measured the diffusion time of the TAMRA-labeled WNK4 peptide using FCS in the presence of different concentrations of GST-fusion proteins of WT and the mutant KLHL3; the binding of KLHL3 to this peptide was assessed by the increased diffusion time of the fluorescent peptide [14,18]. In agreement with our previous study [14], we demonstrated that WT–KLHL3 increased the diffusion time of the TAMRA-labeled peptide (Fig. 3). However, S410L and R528H had little effect on the diffusion time, similar to that observed for GST alone. This indicated that both S410L and R528L decreased the ability to bind to WNK4. Therefore, S410L may have two pathogenic roles in the cells, namely increased degradation and decreased binding to WNK4. These changes may be related to the more severe phenotype of patients with this mutation. For example, Louis-Dit-Picard et al. [10] reported a 29-year-old male patient with a heterozygous S410L mutation, who revealed a blood pressure of 165/98 mm Hg and serum potassium levels of 6.7 mmol/L even under hydrochlorothiazide treatment.

We observed that the behavior of E85A (BTB domain mutant) and C164F (BACK domain mutant) was similar to that of
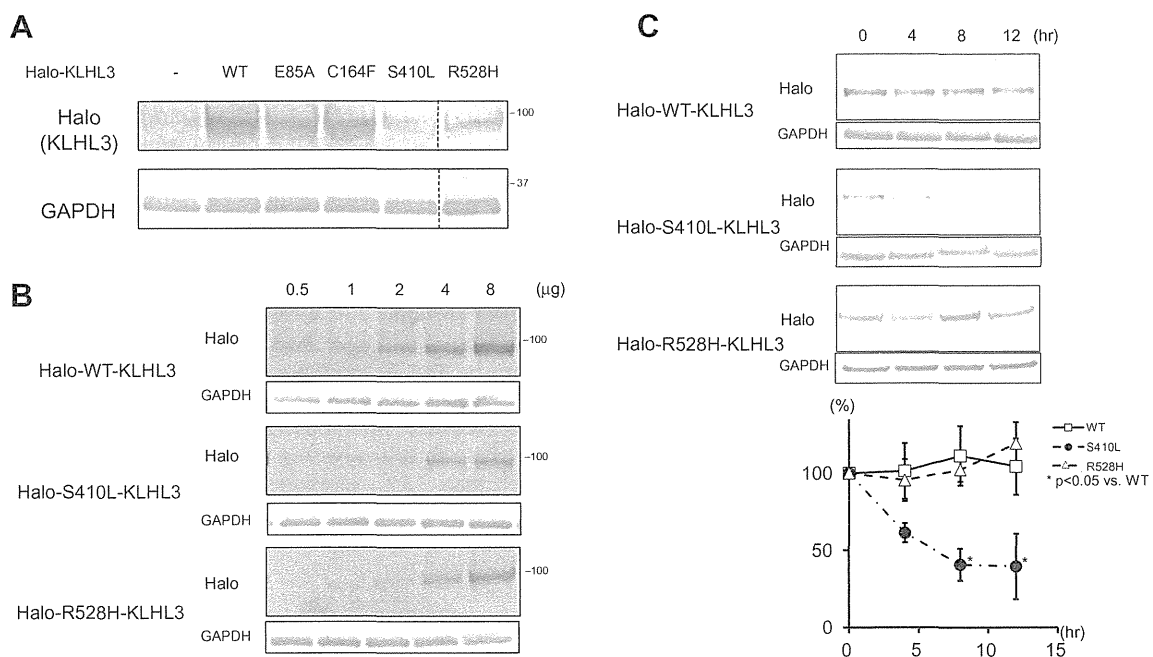

Fig. 2. Transient expression and stability assay of Halo-tagged KLHL3 mutants in the HEK239T cells. (A) We transfected HEK293T cells (1 × 10⁵ cells/3.5-cm dish) with a Halo-KLHL3-pFN21A vector (using 2 μg plasmid). The expression levels of S410L and R528H appeared to be lower compared with those for the other genes. (B) Wild-type, S410L, and R528H KLHL3 were expressed in HEK293T cells (1 × 10⁵ cells/3.5-cm dish) by different amounts of the expression plasmids. The expression of S410L and R528H was lower compared with that of the wild-type KLHL3. (C) Cycloheximide chase assay of Halo-WT-KLHL3, Halo-S410L-KLHL3, and Halo-R528H-KLHL3. Halo-S410L-KLHL3 was degraded more rapidly compared with Halo-WT-KLHL3 and Halo-R528H-KLHL3. The half-life of Halo-S410L-KLHL3 was approximately 6 h.
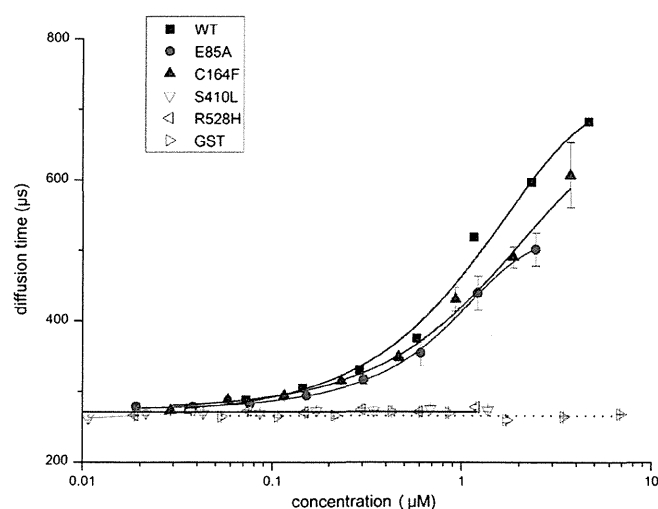
Fig. 3. FCS assay of the binding of KLHL3 and WNK4. The diffusion time of the TAMRA-labeled WNK4 peptide containing the acidic motif (a binding domain to KLHL3) was measured using FCS in the presence of different concentrations of GST fusion proteins of the wild-type and the KLHL3 mutant. The WNK4 peptide bound to the wild-type, E85A, and C164F GST-KLHL3. On the other hand, GST alone and S410L and R528H did not affect the diffusion time, indicating that these mutants could not bind to WNK4.

WT–KLHL3 in the FCS assay, indicating that these mutants maintained the ability to bind to WNK4. This result was not unexpected because the BTB and BACK domains of KLHL proteins are both thought to be involved in binding, not to the substrates (WNK kinases) but to CUL3 [17,21,22]. As presented in Supplementary Fig. 1, we confirmed the decreased binding of these mutants to CUL3 using a coimmunoprecipitation experiment.

3.4. Decreased ability of KLHL3 mutants causing PHAII to ubiquitinate WNK4 and to decrease the intracellular WNK4 protein levels

We previously reported that the expression of WT–KLHL3 significantly decreased the coexpressed protein levels of WNK4, but this effect of KLHL3 was impaired in a PHAII-causing R528H mutant [14]. Wu et al. recently reported a similar effect in other mutants associated with PHAII, including R528H and C164F, in Xenopus oocytes [16]. As presented in Fig. 4A, coexpression of PHAII-causing mutants revealed less ability to decrease the intracellular WNK4 protein levels compared with that of WT–KLHL3. Therefore, we performed in vitro and in vivo assays to evaluate WNK4 ubiquitination using the KLHL3 mutants E85A, C164F, and S410L. We have previously demonstrated that the GST-WNK4-His protein (residue from 490 to 626 containing the binding domain to KLHL3) was directly ubiquitinated by the KLHL3–CUL3 complex in vitro and that the R528H mutation caused a significant decrease in WNK4 ubiquitination [14]. Further, as presented in Fig. 4B, the ability of the mutant KLHL3–CUL3 complexes (E85A, C164F, and S410L) to ubiquitinate WNK4 was lesser compared with that of the wild-type KLHL3. In addition, we performed an in vivo ubiquitination assay to confirm this finding. Following the coexpression of FLAG-tagged WNK4, Halo-tagged KLHL3, and hemagglutinin (HA)-tagged ubiquitin in HEK293T cells, the cells were treated with 1 μM epoxomicin, and WNK4 immunoprecipitated with the FLAG antibody. In order to exclude the ubiquitination signals from other proteins that coimmunoprecipitated with WNK4, immunoprecipitation was performed under denaturing conditions. The ubiquitination signals were observed as a smear band of over approximately 200 kDa, which is the apparent molecular size of
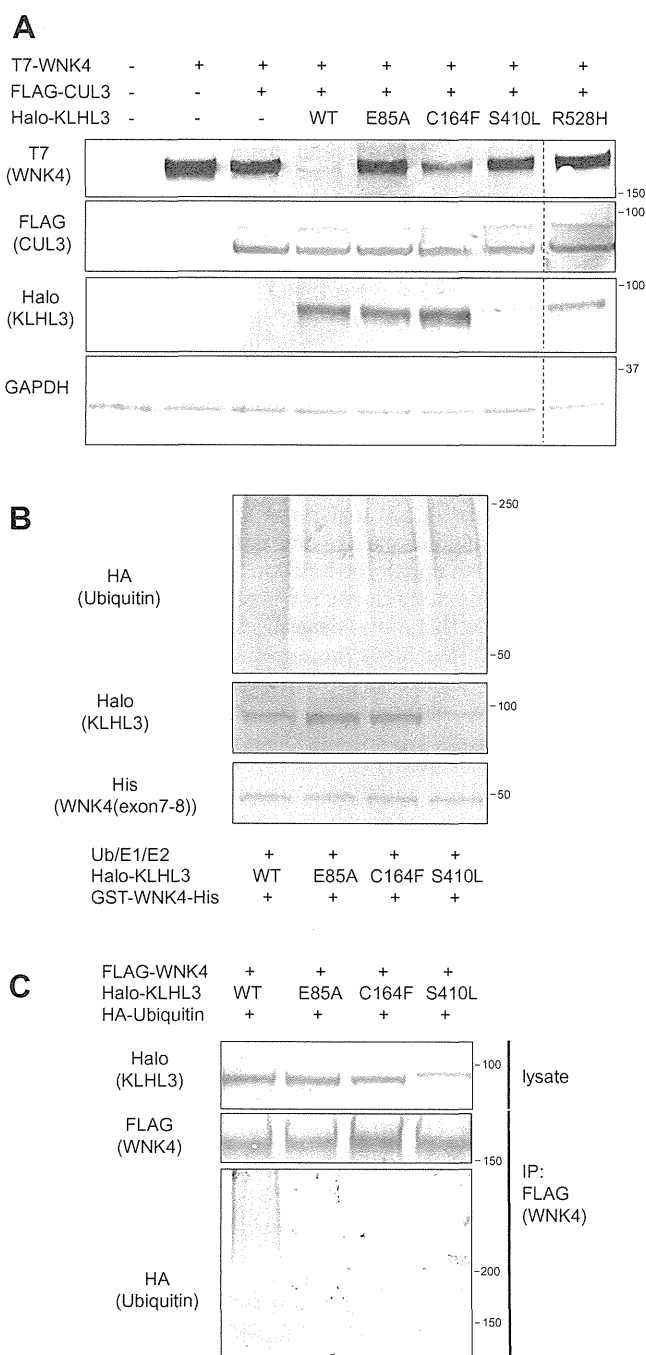

Fig. 4. Effect of the wild-type and mutant KLHL3 on the protein levels and ubiquitination of WNK4. (A) T7-tagged WNK4 and FLAG-tagged CUL3 were coexpressed with Halo-tagged KLHL3. Coexpression of the wild-type KLHL3 caused a significant decrease in the abundance of WNK4, but the KLHL3 mutants were less able to reduce WNK4. (B) In vitro ubiquitination assay of WNK4. As demonstrated in our previous report (14, 18), the wild-type KLHL3 complex ubiquitinated the GST-WNK4-His protein. However, the KLHL3 mutant failed to ubiquitinate WNK4 as efficiently as wild-type KLHL3. (C) In vivo ubiquitination assay of WNK4. Wild-type KLHL3 coexpression increased the WNK4 ubiquitination. However, the KLHL3 mutants were less able to ubiquitinate WNK4.

WNK4. As presented in Fig. 4C, WNK4 ubiquitination by these KLHL3 mutants was lower compared with that by WT–KLHL3.

Following our publication that impaired WNK4 ubiquitination was a common molecular mechanism in PHAII and was caused by mutations in WNK4 (D564A), KLHL3 (R528H), and CUL3 (skipping of exon 9), Shibata et al. analyzed the same R528H mutant

and reported similar results [15]. In addition to R528H, Wu et al. examined other PHAII-causing mutants (A77E, C164F, Q309R, and L387P) in Xenopus oocytes and confirmed that they were less effective in decreasing the WNK4 protein levels compared with WT–KLHL3 [16]. However, with the exception of R528H, the effect of these mutations on WNK4 ubiquitination has not been investigated. A more thorough investigation of these disease-causing mutants of the KLHL3 gene is therefore necessary to establish the pathogenesis of PHAII. Evidence to date indicates these mutations are distributed in different functional domains of the KLHL3 protein and that KLHL proteins other than E3 ligase (e.g., actin-binding protein) may have a pathogenic role in PHAII [10]. The current study clearly demonstrated that each mutation associated with PHAII led to the common consequence of decreased WNK4 ubiquitination, with this effect being mediated through different molecular mechanisms. The mutations in the BTB and BACK domains affected the interaction with CUL3, whereas those in the Kelch domains affected the binding to WNK4. In addition to the impaired binding to WNK4 or CUL3, analysis of S410L in this study suggested that some mutants may be unstable within the cells, which would be expected to impair the functions of KLHL3. Therefore, the data obtained in this study clearly establishes that impaired WNK4 ubiquitination by KLHL3 mutations causes PHAII. Recently, we reported that KLHL2, the KLHL protein member that is closest to KLHL3, could also behave as an E3-ubiquitine ligase with CUL3 [18]. In addition, we observed that KLHL2 had the ability to bind to all WNK kinases, although Ohta et al. reported that KLHL3 could bind and ubiquitinate WNK1 [17]. In this regard, the regulation of WNK kinases by KLHL2 and KLHL3 may occur in various types of cells in the body and may be involved not only in the pathogenesis of PHAII but also in other pathophysiological conditions.

In summary, we clarified the pathogenic mechanisms of PHAII-causing mutations in different domains in KLHL3. Although the molecular mechanisms were different, impaired WNK4 ubiquitination is a common consequence of these mutations.

Acknowledgments

Appendix A. Supplementary data

Supplementary data associated with this article can be found, in the online version, at http://dx.doi.org/10.1016/j.bbrc.2013.08.035.

References

[1] R.D. Gordon, The syndrome of hypertension and hyperkalemia with normal glomerular filtration rate: Gordon's syndrome, Aust. NZ J. Med. 16 (1986) 183–184.

[2] F.H. Wilson, S. Disse-Nicodeme, K.A. Choate, K. Ishikawa, C. Nelson-Williams, I. Desitter, M. Gunel, D.V. Milford, G.W. Lipkin, J.M. Achard, M.P. Feely, B. Dussol, Y. Berland, R.J. Unwin, H. Mayan, D.B. Simon, Z. Farfel, X. Jeunemaitre, R.P. Lifton, Human hypertension caused by mutations in WNK kinases, Science 293 (2001) 1107–1112.

[3] C. Richardson, D.R. Alessi, The regulation of salt transport and blood pressure by the WNK-SPAK/OSR1 signalling pathway, J. Cell Sci. 121 (2008) 3293–3304.

[4] J.A. McCormick, D.H. Ellison, The WNKs: atypical protein kinases with pleiotropic actions, Physiol. Rev. 91 (2011) 177–219.

[5] S.S. Yang, T. Morimoto, T. Rai, M. Chiga, E. Sohara, M. Ohno, K. Uchida, S.H. Lin, T. Moriguchi, H. Shibuya, Y. Kondo, S. Sasaki, S. Uchida, Molecular pathogenesis of pseudohypoaldosteronism type II: generation and analysis of a WNK4 (D561A/+) knockin mouse model, Cell Metab. 5 (2007) 331–344.

[6] M. Chiga, T. Rai, S.S. Yang, A. Ohta, T. Takizawa, S. Sasaki, S. Uchida, Dietary salt regulates the phosphorylation of OSR1/SPAK kinases and the sodium chloride cotransporter through aldosterone, Kidney Int. 74 (2008) 1403–1409.

[7] A. Ohta, T. Rai, N. Yui, M. Chiga, S.S. Yang, S.H. Lin, E. Sohara, S. Sasaki, S. Uchida, Targeted disruption of the WNK4 gene decreases phosphorylation of Na–Cl cotransporter, increases Na excretion and lowers blood pressure, Hum. Mol. Genet. 18 (2009) 3978–3986.

[8] M. Chiga, F.H. Rafiqi, D.R. Alessi, E. Sohara, A. Ohta, T. Rai, S. Sasaki, S. Uchida, Phenotypes of pseudohypoaldosteronism type II caused by the WNK4 D561A missense mutation are dependent on the WNK-OSR1/SPAK kinase cascade, J. Cell Sci. 124 (2011) 1391–1395.

[9] L.M. Boyden, M. Choi, K.A. Choate, C.J. Nelson-Williams, A. Farhi, H.R. Toka, I.R. Tikhonova, R. Bjornson, S.M. Mane, G. Colussi, M. Lebel, R.D. Gordon, B.A. Semmekrot, A. Poujol, M.J. Valimaki, M.E. De Ferrari, S.A. Sanjad, M. Gutkin, F.E. Karet, J.R. Tucci, J.R. Stockigt, K.M. Keppler-Noreuil, C.C. Porter, S.K. Anand, M.L. Whiteford, I.D. Davis, S.B. Dewar, A. Bettinelli, J.J. Fadrowski, C.W. Belsha, T.E. Hunley, R.D. Nelson, H. Trachtman, T.R. Cole, M. Pinsk, D. Bockenhauer, M. Shenoy, P. Vaidyanathan, J.W. Foreman, M. Rasoulpour, F. Thameem, H.Z. Al-Shahrouri, J. Radhakrishnan, A.G. Gharavi, B. Goilav, R.P. Lifton, Mutations in Kelch-like 3 and Cullin3 cause hypertension and electrolyte abnormalities, Nature 482 (2012) 98–102.

[10] H. Louis-Dit-Picard, J. Barc, D. Trujillano, S. Miserey-Lenkei, N. Bouatia-Naji, O. Pylypenko, G. Beaurain, A. Bonnefond, O. Sand, C. Simian, E. Vidal-Petiot, C. Soukaseum, C. Mandet, F. Broux, O. Chabre, M. Delahousse, V. Esnault, B. Fiquet, P. Houillier, C.J. Bagnis, J. Koenig, M. Konrad, P. Landais, C. Mourani, P. Niaudet, V. Probst, C. Thauvin, R.J. Unwin, S.D. Soroka, G. Ehret, S. Ossowski, M. Caulfield, P. Bruneval, X. Estivill, P. Froguel, J. Hadchouel, J.J. Schott, X. Jeunemaitre, I.C.f.B.P. (ICBP), KLHL3 mutations cause familial hyperkalemic hypertension by impairing ion transport in the distal nephron, Nat. Genet. 44 (2012) 456–460. S451–453.

[11] M. Furukawa, Y. Xiong, BTB protein keap1 targets antioxidant transcription factor Nrf2 for ubiquitination by the Cullin3-Roc1 ligase, Mol. Cell Biol. 25 (2005) 162–171.

[12] Y.R. Lee, W.C. Yuan, H.C. Ho, C.H. Chen, H.M. Shih, R.H. Chen, The Cullin3 substrate adaptor KLHL20 mediates DAPK ubiquitination to control interferon responses, EMBO J. 29 (2010) 1748–1761.

[13] M.Y. Lin, Y.M. Lin, T.C. Kao, H.H. Chuang, R.H. Chen, PDZ-RhoGEF ubiquitination by Cullin3-KLHL20 controls neurotrophin-induced neurite outgrowth, J. Cell Biol. 193 (2011) 985–994.

[14] M. Wakabayashi, T. Mori, K. Isobe, E. Sohara, K. Susa, Y. Araki, M. Chiga, E. Kikuchi, N. Nomura, Y. Mori, H. Matsuo, T. Murata, S. Nomura, T. Asano, H. Kawaguchi, S. Nonoyama, T. Rai, S. Sasaki, S. Uchida, Impaired KLHL3-mediated ubiquitination of WNK4 causes human hypertension, Cell Rep. 3 (2013) 858–868.

[15] S. Shibata, J. Zhang, J. Puthumana, K.L. Stone, R.P. Lifton, Kelch-like 3 and Cullin3 regulate electrolyte homeostasis via ubiquitination and degradation of WNK4, Proc. Natl. Acad. Sci. USA 110 (2013) 7838–7843.

[16] G. Wu, J.B. Peng, Disease-causing mutations in KLHL3 impair its effect on WNK4 degradation, FEBS Lett. (2013).

[17] A. Ohta, F.R. Schumacher, Y. Mehellou, C. Johnson, A. Knebel, T.J. Macartney, N.T. Wood, D.R. Alessi, T. Kurz, The CUL3–KLHL3 E3 ligase complex mutated in Gordon's hypertension syndrome interacts with and ubiquitylates WNK isoforms: disease-causing mutations in KLHL3 and WNK4 disrupt interaction, Biochem. J. 451 (2013) 111–122.

[18] D. Takahashi, T. Mori, M. Wakabayashi, Y. Mori, K. Susa, M. Zeniya, E. Sohara, T. Rai, S. Sasaki, S. Uchida, KLHL2 interacts with and ubiquitinates WNK kinases, Biochem. Biophys. Res. Commun. (2013).

[19] K. Yamauchi, T. Rai, K. Kobayashi, E. Sohara, T. Suzuki, T. Itoh, S. Suda, A. Hayama, S. Sasaki, S. Uchida, Disease-causing mutant WNK4 increases paracellular chloride permeability and phosphorylates claudins, Proc. Natl. Acad. Sci. USA 101 (2004) 4690–4694.

[20] K. Kuroki, S. Kobayashi, M. Shiroishi, M. Kajikawa, N. Okamoto, D. Kohda, K. Maenaka, Detection of weak ligand interactions of leukocyte Ig-like receptor B1 by fluorescence correlation spectroscopy, J. Immunol. Methods 320 (2007) 172–176.

[21] A.X. Ji, G.G. Privé, Crystal Structure of KLHL3 in complex with Cullin3, PLoS One 8 (2013) e60445.

[22] Y. Kigoshi, F. Tsuruta, T. Chiba, Ubiquitin ligase activity of CUL3–KLHL7 protein is attenuated by autosomal dominant retinitis pigmentosa causative mutation, J. Biol. Chem. 286 (2011) 33613–33621.
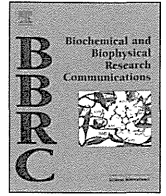
Treatment with 17-allylamino-17-demethoxygeldanamycin ameliorated symptoms of Bartter syndrome type IV caused by mutated *Bsnd* in mice

Naohiro Nomura [a], Kazusaku Kamiya [b], Katsuhisa Ikeda [b], Naofumi Yui [a], Motoko Chiga [a], Eisei Sohara [a], Tatemitu Rai [a], Sei Sakaki [a], Shinich Uchida [a,*]

[a] Department of Nephrology, Graduate School of Medical and Dental Sciences, Tokyo Medical and Dental University, 1-5-45 Yushima, Bunkyo-ku, Tokyo 113-8519, Japan
[b] Department of Otorhinolaryngology, Juntendo University Faculty of Medicine, 2-1-1 Hongo, Bunkyo-ku, Tokyo 113-8421, Japan

ABSTRACT

Mutations of *BSND*, which encodes barttin, cause Bartter syndrome type IV. This disease is characterized by salt and fluid loss, hypokalemia, metabolic alkalosis, and sensorineural hearing impairment. Barttin is the β-subunit of the ClC-K chloride channel, which recruits it to the plasma membranes, and the ClC-K/barttin complex contributes to transepithelial chloride transport in the kidney and inner ear. The retention of mutant forms of barttin in the endoplasmic reticulum (ER) is etiologically linked to Bartter syndrome type IV. Here, we report that treatment with 17-allylamino-17-demethoxygeldanamycin (17-AAG), an Hsp90 inhibitor, enhanced the plasma membrane expression of mutant barttins (R8L and G47R) in Madin–Darby canine kidney cells. Administration of 17-AAG to $Bsnd^{R8L/R8L}$ knock-in mice elevated the plasma membrane expression of R8L in the kidney and inner ear, thereby mitigating hypokalemia, metabolic alkalosis, and hearing loss. These results suggest that drugs that rescue ER-retained mutant barttin may be useful for treating patients with Bartter syndrome type IV.

© 2013 Elsevier Inc. All rights reserved.

1. Introduction

Mutations of *BSND* that encode barttin cause Bartter syndrome type IV [1]. This disease is characterized by salt and fluid loss, hypokalemia, metabolic alkalosis, and sensorineural hearing impairment. Patients with Bartter syndrome are typically treated with potassium-sparing diuretics such as spironolactone or amiloride, angiotensin inhibitors, and potassium supplementation and frequently treated with nonsteroidal anti-inflammatory drugs to suppress the elevation of renal prostaglandin E2. However, these treatments only partially ameliorate Bartter syndrome symptoms. Sensorineural hearing impairment accompanies renal symptoms; however, no treatment is available for this impairment.

Barttin is the β-subunit of ClC-K chloride channels that are expressed in the distal renal tubules and inner ear [2]. Barttin is coexpressed with ClC-K1 in apical and basolateral membranes of the thin ascending limb of Henle's loop [3,4] and with ClC-K2 in the basolateral plasma membranes of nephron segments from the thick ascending limb of Henle's loop to intercalated cells in collecting ducts [5–7]. Constitutive barttin knockout mice die a few days after birth because of severe dehydration [8]. Moreover, barttin hypomorphic mice suffer from severe polyuria,

hypokalemia, and metabolic alkalosis [9]. These findings indicate that ClC-K/barttin plays a crucial role in transepithelial chloride transport in the kidney.

Barttin colocalizes with ClC-K1 and ClC-K2 in the basolateral membrane of marginal cells of the stria vascularis and vestibular dark cells [2]. Mechanical vibration is enhanced and converted to electrical signals through outer and inner hair cells in the organ of Corti. To allow a depolarizing influx of potassium ions through apical mechanosensitive cation channels of hair cells, the endolymph that fills the cavity of the scala media is high in K^+ and has a positive potential [10,11]. These conditions are generated by the stria vascularis, which comprises a multilayered epithelium [11,12]. Inner ear-specific barttin knockout mice show a significant decrease of endocochlear potential (EP) and are congenitally deaf [8], indicating that barttin/ClC-K is required to generate EP.

Patients with Bartter syndrome type IV harbor different *BSND* mutations [1,13–20]. The R8L missense mutant barttin does not activate the ClC-K chloride channel currents when introduced into *Xenopus laevis* oocytes, and R8L barttin and C1C-K are not expressed on the plasma membrane [2,21]. We showed that the R8L barttin stably expressed in Madin–Darby canine kidney (MDCK) cells was trapped in the endoplasmic reticulum (ER) and did not reach the plasma membrane [22]. Recently, we confirmed this phenotype in the kidneys of $Bsnd^{R8L/R8L}$ knock-in mice (R8L knock-in mice) [9].

---

* Corresponding author. Fax: +81 3 5803 5215.
  E-mail address: suchida.kid@tmd.ac.jp (S. Uchida).

Certain pathogenic proteins are misfolded and are retained in the ER, including the cystic fibrosis transmembrane conductance regulator (CFTR) [23–26], aquaporin 2 (AQP2) [27,28], V2 vasopressin receptor [29,30], podocin [31], and Tamm–Horsfall Protein (THP) [32]. Attempts have been made to rescue these ER-trapped mutant proteins. For example, the Hsp90 inhibitor 17-allylamino-17-demethoxygeldanamycin (17-AAG) increases cell-surface expression of AQP2-T125 M and partially corrects nephrogenic diabetes insipidus phenotype in AQP2$^{T126M/-}$ mice [28]. Moreover, 17-AAG increases the stability of mutant pendrin by inhibiting its ubiquitin-mediated degradation [33].

In the present study, we investigated the effect of 17-AAG treatment on mislocalized R8L barttin in MDCK cells and in R8L knock-in mice. We found that 17-AAG increased the expression of R8L barttin on the plasma membrane and partially ameliorated the phenotypes of Bartter syndrome type IV, including hearing loss.

2. Material and methods

2.1. Cell culture and analysis of cell-surface expression of barttin

We used MDCK cells stably expressing wild-type (WT) and R8L mutant barttin, which are described in our previous study [22]. G47R mutant barttin stably expressing MDCK cells were generated with site-directed mutagenesis and G418 selection as previously described [22]. Cell-surface proteins were harvested using a published side-specific biotinylation technique [34]. MDCK cells were incubated in the wells of 6-well TransWell filters (Corning) for at least 3 days to form confluent monolayers and were then incubated with 17-AAG (LC Laboratories), curcumin (Sigma–Aldrich), trimethylamine oxide (TMAO) (Sigma–Aldrich), or DMSO (0.15%) as control for 2 h before biotinylation. Cells were biotinylated using EZ-Link Sulfo-NHS-SS-biotin (Thermo Scientific) for 30 min. After quenching the remaining biotin with 50 mM NH₄Cl, cells were lysed with lysis buffer (150 mM NaCl, 20 mM Tris–HCl, 5 mM EDTA, and 1% Trion-X-100). Biotinylated proteins were bound to NeutrAvidin resin (Thermo Scientific), eluted using sodium dodecyl sulfate polyacrylamide gel electrophoresis (SDS–PAGE) buffer containing 50 mM dithiothreitol at 60 °C for 20 min and then subjected to immunoblotting. Blots were incubated with an anti-barttin antibody diluted to 1:200 with 5% skim milk in Tris-buffered saline with tween (TBST) [9]. Immunofluorescence (IF) detection of barttin in MDCK cells grown on filters was performed as follows. The cells were fixed with 3% paraformaldehyde (PFA) for 15 min, permeabilized with 0.1% Triton X-100 in PBS for 10 min, blocked in 1% bovine serum albumin (BSA) in phosphate buffered saline (PBS) for 30 min, and then incubated with the anti-barttin antibody (1:200 dilution with 1% BSA in PBS) for 2 h at room temperature. Alexa-Fluor®-labeled secondary antibodies (Life Technologies) were used to detect the barttin-primary antibody complexes. IF images were observed using an LSM510 Meta fluorescence microscope (Carl Zeiss).
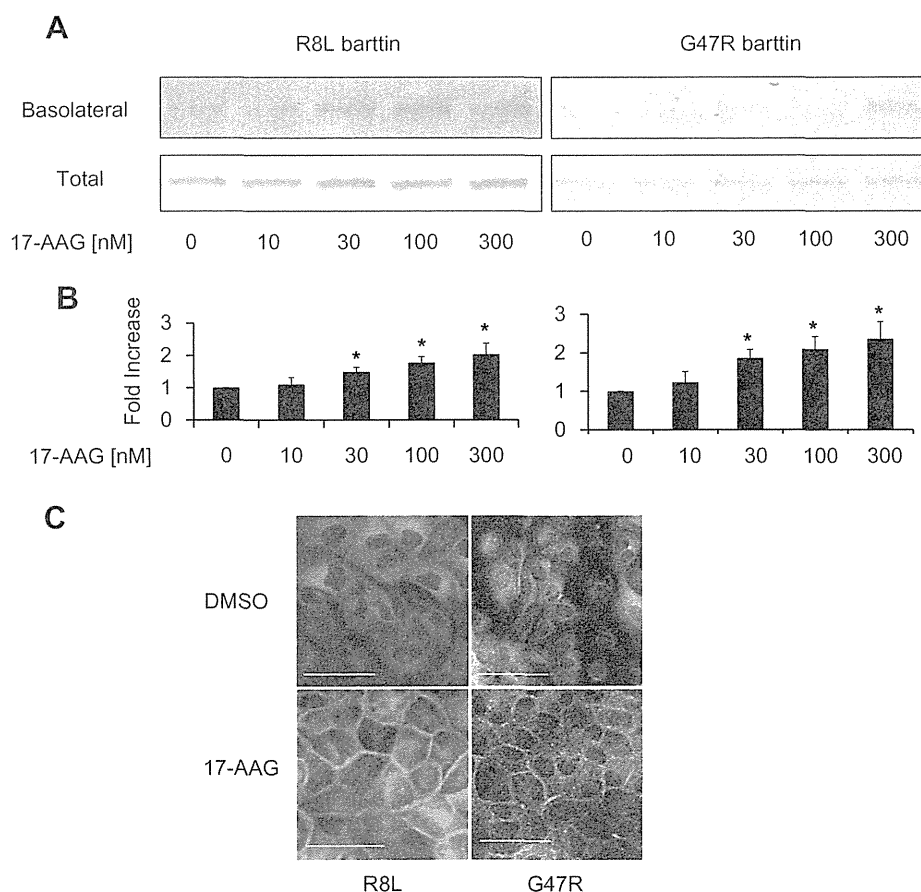

Fig. 1. Effect of 17-allylamino-17-demethoxygeldanamycin (17-AAG) on cell-surface expression of R8L and G47R mutant barttins R8L and G47R were stably expressed in Madin–Darby canine kidney (MDCK) cells. The cells were incubated with 17-AAG 2 h before biotin labeling and IF analysis. (A) Expression of R8L and G47R in basolateral plasma membranes increased after treatment with >30 nM 17-AAG. (B) Densitometric analyses of the data shown in Fig. 1A. N = 4 (R8L), N = 3 (G47R), *p < 0.05. (C) Immunofluorescence analysis of R8L and G47R showing increased expression on the plasma membrane after treatment with 17-AAG (300 nM). At least three independent experiments yielded similar results. Scale bars = 50 μM.
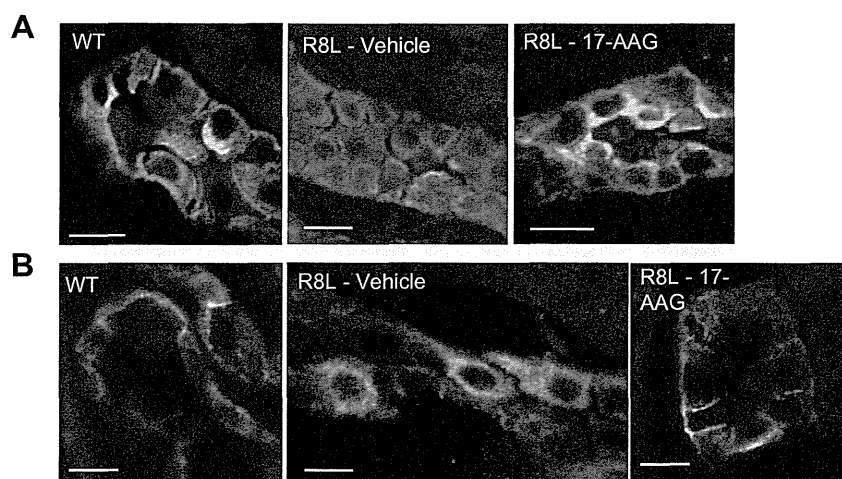
Fig. 2. Representative images of R8L barttin and ClC-K in the kidney of an R8L knock-in mice after 17-allylamino-17-demethoxygeldanamycin (17-AAG) treatment 17-AAG (25 mg/kg) or dimethyl sulfoxide (DMSO; vehicle control) was intraperitoneally administered. (A) 17-AAG restored the plasma membrane localization of R8L barttin (red) in connecting tubules. Apical green staining identifies AQP2. (B) Localization of ClC-K in intercalated cells in the cortical connecting duct was corrected by 17-AAG treatment in R8L knock-in mice. WT: wild-type mice, R8L: R8L knock-in mice. Scale bars = 10 μm. (For interpretation of the references to colour in this figure legend, the reader is referred to the web version of this article.)

Table 1
Analysis of blood samples obtained from R8L knock-in mice before and after17-allylamino-17-demethoxygeldanamycin (17-AAG) treatment.

	DMSO + Low NaCl diet ($N = 10$)		17-AAG + Low NaCl diet ($N = 9$)	
	Before treatment (regular)	After treatment (low NaCl)	Before treatment (regular)	After treatment (low NaCl)
Na (mEq/L)	147 ± 0	143 ± 1	146 ± 1	142 ± 1
K (mEq/L)	4.5 ± 0.2	3.9 ± 0.2	4.7 ± 0.1	4.5 ± 0.1
Cl (mEq/L)	111 ± 1	106 ± 1	111 ± 1	108 ± 1
pH	7.294 ± 0.015	7.345 ± 0.016	7.285 ± 0.012	7.321 ± 0.018
HCO_3^- (mEq/L)	22.8 ± 0.4	25.6 ± 0.6	22.6 ± 0.4	24.1 ± 0.8

The knock-in mice were injected with 17-allylamino-17-demethoxygeldanamycin (17-AAG) (25 mg/kg) or dimethyl sulfoxide (DMSO; vehicle control) daily for 7 days. The mice were fed a low salt diet during treatment. Plasma HCO_3^- levels and pH of DMSO-treated mice fed a low salt diet increased. However, the increase of plasma HCO_3^- and pH in 17-AAG-treated mice was not significant. DMSO-treated mice fed a low salt diet were hypokalemic; however, 17-AAG-treated mice were not.
* $p < 0.05$ vs. Pre.
† $p < 0.05$ vs. DMSO. Na, sodium; K, potassium; Cl, chloride; HCO_3^-, bicarbonate.

2.2. Immunofluorescent analysis of mouse tissues

The Animal Care and Use Committee of Tokyo Medical and Dental University approved the experiments conducted using animals. Mice were intraperitoneally administered 17-AAG (25 mg/kg) 2 h before tissue preparation. 17-AAG was dissolved in 50% DMSO, and the same volume of 50% DMSO was used as a vehicle control. Tissues were prepared as described previously [35]. Mice were deeply anesthetized with ether, and tissues were harvested and fixed with 4% PFA in PBS by perfusion through the left ventricle. The kidneys were removed and placed in the fixative. To prepare inner ear specimens, the temporal bones were removed and placed in the fixative. Small openings were made at the round and oval windows and at the apex of the cochlea, and the perilymphatic space was then gently perfused with fixative. After 1 h, the right temporal bones were decalcified by immersion in 5% ethylenedi-aminetetraacetic acid with stirring at 4 °C for approximately 7 days. Kidney and right inner-ear specimens were soaked for several hours in 20% sucrose in PBS, embedded in Tissue-Tek OCT compound (Sakura Finetechvical Co., Ltd.), and snap frozen. For whole-mount staining of the stria vascularis, fixed left-inner ears were microdissected, and the isolated stria vascularis was soaked in fixative. The whole-mount samples were treated with 0.5% Triton X-100 in PBS for 30 min. Frozen sections and whole-mount samples were blocked using 1% BSA in PBS and incubated with primary antibodies as follows: anti-barttin (diluted 1:200 with 0.1%

BSA in PBS) [9] and anti-ClC-K (diluted 1:100) [36]. The secondary antibodies were conjugated to Alexa-Fluor® (diluted 1:200). Samples were mounted using VECTASHIELD® with DAPI (Vector Laboratories).

2.3. Analysis of blood

Blood was collected from the submandibular vein after administering light anesthesia with ether. Blood data was determined using an i-STAT® analyzer (Fuso, Osaka, Japan). Baseline blood data were acquired from mice fed a normal diet (0.4% NaCl). The mice were then fed a low salt diet (0.01% NaCl) that induces hypokalemia and metabolic alkalosis in R8L barttin knock-in mice. We administered intraperitoneal injections of 25 mg/kg 17-AAG once daily for 7 days. Blood samples were collected after the treatment period. All nutrients were obtained from the Oriental Yeast Co., Ltd., (Tokyo, Japan).

2.4. Auditory brainstem response (ABR)

ABR recording was performed as previously described [35]. Mice were anesthetized using pentobarbital before placing stainless steel needle electrodes dorsolaterally to the ears. Waveforms of 512 stimuli (9 Hz) were averaged, and the visual detection threshold was determined using varying sound pressure levels. Baseline hearing thresholds were recorded first. After 2 h of
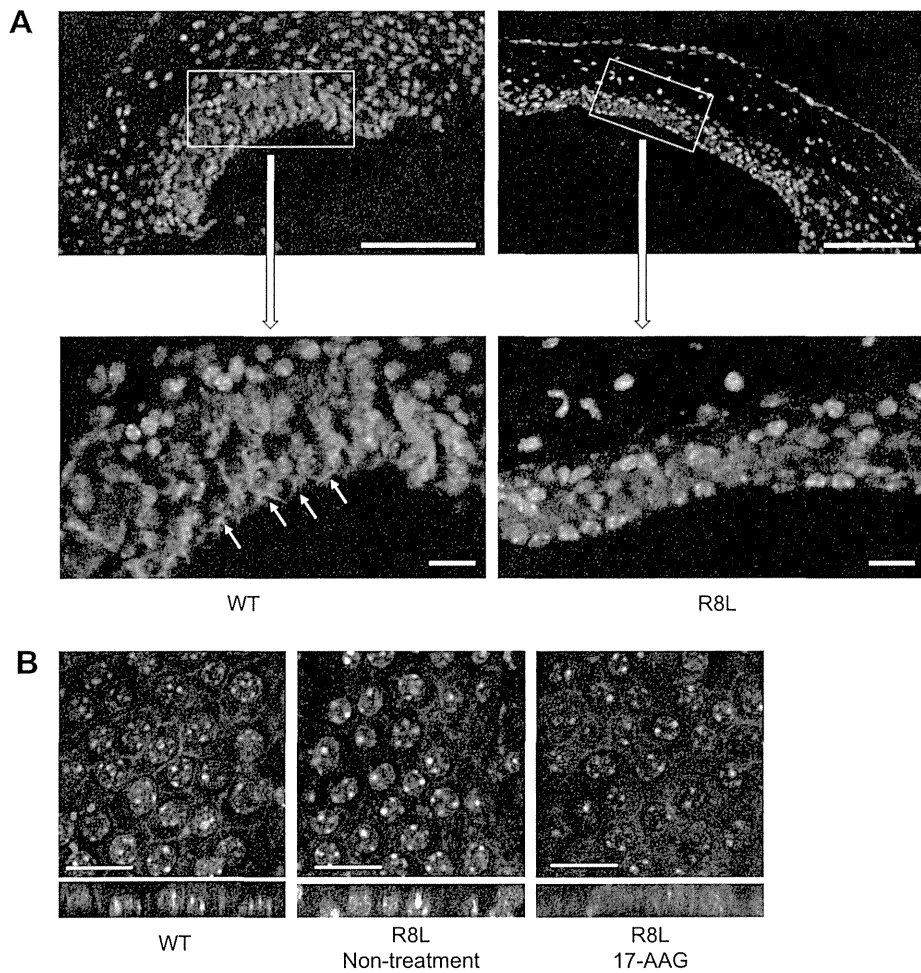
Fig. 3. Representative images of barttin in the stria vascularis. (A) Representative images of barttin in frozen sections of the stria vascularis. Wild-type (WT) barttin appeared to be present on the lateral walls of marginal cells (arrows), whereas R8L expression on the plasma membrane was not clear. Blue indicates nuclear (DAPI) staining. Scale bars = 100 μm in upper panels, 20 μm in lower panels. (B) Representative images of barttin (red) in whole mounts of the stria vascularis. Blue indicates nuclear (DAPI) staining. Scale bars = 20 μm. Lower panels show z-stacks of upper panels. Wild-type (WT) barttin was observed on the lateral walls of marginal cells (left panel), whereas R8L expression on the plasma membrane was not clear (middle panel). 17-AAG treatment partially restored the plasma membrane expression of R8L (right panel). (For interpretation of the references to colour in this figure legend, the reader is referred to the web version of this article.)

Table 2
Hearing thresholds (dB) of wild-type (WT) and R8L knock-in mice assessed using auditory brainstem response (ABR).

Frequency		3-Week-old mice	5-Week-old mice	10-Week-old mice
8000 Hz	WT	16.0 ± 2.0	19.9 ± 1.7	21.8 ± 1.4
	R8L	36.0 ± 2.8	54.9 ± 2.9 [†]	70.4 ± 3.3 [†§]
20,000 Hz	WT	6.7 ± 2.3	14.1 ± 2.8	13.4 ± 0.0
	R8L	42.6 ± 5.5	50.9 ± 2.0	63.4 ± 2.9 [†§]

The numbers of mice are shown in Fig. 4A.
[*] $p < 0.05$ vs. WT.
[†] $p < 0.05$, 3-week-old mice.
[§] $p < 0.05$, 5-week-old mice.

recovery from anesthesia, 17-AAG (25 mg/kg) or vehicle (equal volume of 50% DMSO) was intraperitoneally injected and hearing thresholds were determined again.

2.5. Statistical methods

All values are expressed as the mean ± standard error of the mean (SE). Statistical analyses of the effects of treatment were performed using a paired t-test. Other statistical analyses were performed using an unpaired t-test. p-Values <0.05 were considered statistically significant.

3. Results

3.1. Cell-surface expression of mutant barttins by MDCK cells is increased by treatment with 17-AAG

Analysis of MDCK cells stably expressing human R8L and G47R barttins showed that barttin localization was primarily intracellular (Fig. 1). We next tested whether agents that rescue ER-trapped mutant membrane proteins (17-AAG, curcumin, and TMAO) [23,25,26,28,33] were effective in relocalizing the mutant barttins. IF and site-specific biotin labeling revealed that these agents effectively increased the basolateral plasma membrane expression of the mutant proteins (Fig. 1 and Fig. S1). Moreover, the basolateral expression of WT barttin did not increase in response to 17-AAG (Fig. S2). We also assessed the effects of 17-AAG on barttin mutants G10S, I12T, Q32X; however, G10S and I12T mutant barttin were expressed on the plasma membrane before the treatment [17,22,37], and the low level of Q32X barttin expression did not permit the acquisition of meaningful data.

3.2. Partial rescue of renal phenotypes of R8L knock-in mice

We previously showed that R8L and ClC-K expression in the basolateral membrane is significantly decreased in the renal
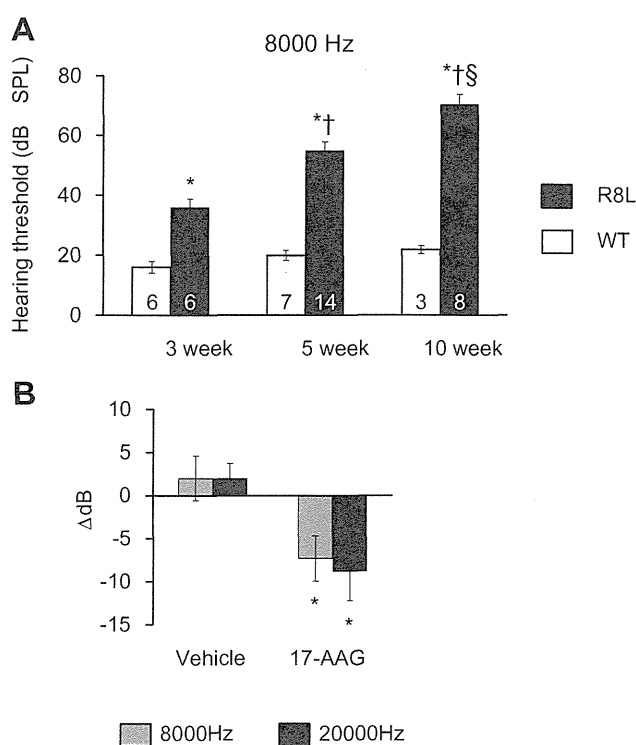
Fig. 4. Hearing impairment in R8L knock-in mice and its amelioration with 17-AAG treatment (A) Hearing thresholds at 8000 Hz in wild-type (WT) and R8L knock-in mice measured using auditory brainstem response (ABR). Numbers of mice are shown on the columns. *$p < 0.05$ vs. WT, [†]$p < 0.05$ vs. 3-week-old mice, [§]$p < 0.05$ vs. 5-week-old mice. (B) Variation of hearing thresholds before and after treatment. 17-allylamino-17-demethoxygeldanamycin (17-AAG): $N = 13$; vehicle: $N = 10$. *$p < 0.05$ vs. vehicle.

tubules of R8L knock-in mice [9]. IF analysis of the R8L mutants shows that 17-AAG restored the basolateral localization of barttin in the connecting tubules (Fig. 2) and corrected the intracellular localization of ClC-K in the intercalated cells of cortical collecting ducts (Fig. 2).

The R8L knock-in mice suffered from metabolic alkalosis and hypokalemia when fed a low-salt diet [9]. We confirmed our previous findings in the vehicle-treated R8L knock-in mice (Table 1). However, administration of 17-AAG for one week corrected the low salt-induced metabolic alkalosis and ameliorated hypokalemia (Table 1). In wild-type mice, administration of 17-AAG did not significantly affect these parameters (Table S1).

3.3. Partial rescue of sensorineural hearing impairment of R8L knock-in mice

IF analysis revealed that R8L was present in the stria vascularis (Fig. 3A). In higher magnification (lower panels), wild-type barttin appeared to be localized on the lateral walls of marginal cells (arrows), whereas R8L expression on the plasma membrane was not clear. However, it was difficult to assess from this view whether localization of R8L to the plasma membrane was impaired because marginal and intermediate cells are extensively interdigitated. Therefore, we analyzed whole-mount samples (Fig. 3B) and confirmed the finding shown in Fig. 3A. Furthermore, we could observe that 17-AAG treatment partially restored the plasma membrane expression of R8L (Fig. 3B, right panel).

We evaluated hearing impairment using ABR. R8L knock-in mice lost hearing at 8 and 20 kHz compared with control WT littermates at 3-, 6-, and 10-weeks of age (Table 2, Fig. 4A). Although 17-AAG treatment did not affect the hearing thresholds of WT mice (Table S2), it slightly, but significantly, improved the hearing

thresholds of R8L knock-in mice (Fig. 4B). DMSO treatment did not affect hearing thresholds.

4. Discussion

We previously described the renal phenotypes of R8L barttin knock-in mice [9]. Bartter-like phenotypes (loss of salt from the kidney, hypokalemia, and metabolic alkalosis) were only observed when these mice were fed a low salt diet. In contrast to the renal phenotypes, we found here that the hearing of R8L knock-in mice was significantly impaired under normal conditions. Because ABR analysis generated semi-quantitative data indicating impaired function of ClC-K/R8L barttin in vivo, we used this parameter to assess the reversal of symptoms by administering 17-AAG to R8L knock-in mice. We observed significant improvement in the hearing threshold as well as the increased expression of barttin at the plasma membrane. Metabolic alkalosis and hypokalemia were also ameliorated by 17-AAG treatment, which increased the plasma membrane expression of R8L barttin in renal tubules. 17-AAG, a semisynthetic chemical analog of the natural product geldanamycin, inhibits Hsp90 function [38]. Hsp90 participates in a diverse range of cellular processes, including chaperoning of newly synthesized proteins, stress responses, signal transduction, and transcriptional regulation [39]. We chose 17-AAG for the present study because 17-AAG is effective at low concentrations in vitro and has been used in other mouse models of human diseases [28] as well as for treating patients with cancer [40,41]. We previously demonstrated that decreased transepithelial chloride transport and plasma membrane localization of barttin significantly correlate in the thin limb of Henle's loop of R8L knock-in mice, providing compelling evidence that impaired plasma membrane localization of R8L barttin accounts for pathogenesis. We demonstrate that 17-AAG was effective for rerouting barttin to the plasma membrane of MDCK cells expressing R8L and G47R barttin. Therefore, 17-AAG may be useful for treating patients with Bartter syndrome type IV who harbor other BSND missense mutations.

The mechanism underlying the ability of 17-AAG to rescue mutant barttins is unknown. ER-retained mutant barttins may be misfolded and are restored to their native conformations by 17-AAG. This assumption is supported by findings that TMAO and curcumin were also effective in increasing barttin expression at the plasma membrane (Fig. S1). However, it was difficult to confirm this hypothesis from these experiments because the maturation of barttin (an unglycosylated protein) cannot be monitored by its glycosylation. Findings related to those reported here demonstrate that the treatment of human cell lines with 17-AAG facilitates the folding of pendrin through heat shock transcription factor 1-dependent induction of molecular chaperones [33], suggesting that the same mechanism mediates the effects of 17-AAG on R8L and G47R barttin. Restoration from the misfolding by 17-AAG might not only correct the mislocalization of R8L but also decrease ER-associated degradation of R8L, both of which might be involved in the increased plasma membrane expression of R8L by 17-AAG.

In conclusion, we demonstrated that the hearing of patients with Bartter syndrome type IV may be restored by treatment with drugs such as 17-AAG. Further research is required to discover more effective drugs that correct the aberrant intracellular localization of misfolded membrane proteins.

Acknowledgments

Appendix A. Supplementary data

Supplementary data associated with this article can be found, in the online version, at http://dx.doi.org/10.1016/j.bbrc.2013.10.129.

References

[1] R. Birkenhäger, E. Otto, M. Schürmann, M. Vollmer, E. Ruf, I. Maier-Lutz, F. Beekmann, A. Fekete, H. Omran, D. Feldmann, D. Milford, N. Jeck, M. Konrad, D. Landau, N. Knoers, C. Antignac, R. Sudbrak, A. Kispert, F. Hildebrandt, Mutation of BSND causes Bartter syndrome with sensorineural deafness and kidney failure, Nat. Genet. 29 (2001) 310–314.

[2] R. Estévez, T. Boettger, V. Stein, R. Birkenhäger, E. Otto, F. Hildebrandt, T. Jentsch, Barttin is a Cl⁻ channel beta-subunit crucial for renal Cl⁻ reabsorption and inner ear K⁺ secretion, Nature 414 (2001) 558–561.

[3] S. Uchida, S. Sasaki, K. Nitta, K. Uchida, S. Horita, H. Nihei, F. Marumo, Localization and functional characterization of rat kidney-specific chloride channel, ClC-K1, J. Clin. Invest. 95 (1995) 104–113.

[4] S. Uchida, S. Sasaki, T. Furukawa, M. Hiraoka, T. Imai, Y. Hirata, F. Marumo, Molecular cloning of a chloride channel that is regulated by dehydration and expressed predominantly in kidney medulla, J. Biol. Chem. 268 (1993) 3821–3824.

[5] M. Yoshikawa, S. Uchida, A. Yamauchi, A. Miyai, Y. Tanaka, S. Sasaki, F. Marumo, Localization of rat CLC-K2 chloride channel mRNA in the kidney, Am. J. Physiol. 276 (1999) F552–F558.

[6] K. Kobayashi, S. Uchida, S. Mizutani, S. Sasaki, F. Marumo, Intrarenal and cellular localization of CLC-K2 protein in the mouse kidney, J. Am. Soc. Nephrol. 12 (2001) 1327–1334.

[7] S. Adachi, S. Uchida, H. Ito, M. Hata, M. Hiroe, F. Marumo, S. Sasaki, Two isoforms of a chloride channel predominantly expressed in thick ascending limb of Henle's loop and collecting ducts of rat kidney, J. Biol. Chem. 269 (1994) 17677–17683.

[8] G. Rickheit, H. Maier, N. Strenzke, C. Andreescu, C. De Zeeuw, A. Muenscher, A. Zdebik, T. Jentsch, Endocochlear potential depends on Cl⁻ channels: mechanism underlying deafness in Bartter syndrome IV, EMBO J. 27 (2008) 2907–2917.

[9] N. Nomura, M. Tajima, N. Sugawara, T. Morimoto, Y. Kondo, M. Ohno, K. Uchida, K. Mutig, S. Bachmann, M. Soleimani, E. Ohta, A. Ohta, E. Sohara, T. Okado, T. Rai, T.J. Jentsch, S. Sasaki, S. Uchida, Generation and analyses of R8L barttin knockin mouse, Am. J. Physiol. Renal Physiol. 301 (2011) F297–F307.

[10] H. Hibino, Y. Kurachi, Molecular and physiological bases of the K⁺ circulation in the mammalian inner ear, Physiology (Bethesda) 21 (2006) 336–345.

[11] P. Wangemann, Supporting sensory transduction: cochlear fluid homeostasis and the endocochlear potential, J. Physiol. 576 (2006) 11–21.

[12] F. Nin, H. Hibino, K. Doi, T. Suzuki, Y. Hisa, Y. Kurachi, The endocochlear potential depends on two K⁺ diffusion potentials and an electrical barrier in the stria vascularis of the inner ear, Proc. Natl. Acad. Sci. USA 105 (2008) 1751–1756.

[13] Z. Bircan, F. Harputluoglu, N. Jeck, Deletion of exons 2–4 in the BSND gene causes severe antenatal Bartter syndrome, Pediatr. Nephrol. 24 (2009) 841–844.

[14] F. Ozlu, H. Yapicioğlu, M. Satar, N. Narli, K. Ozcan, M. Buyukcelik, M. Konrad, O. Demirhan, Barttin mutations in antenatal Bartter syndrome with sensorineural deafness, Pediatr. Nephrol. 21 (2006) 1056–1057.

[15] N. Miyamura, K. Matsumoto, T. Taguchi, H. Tokunaga, T. Nishikawa, K. Nishida, T. Toyonaga, M. Sakakida, E. Araki, Atypical Bartter syndrome with sensorineural deafness with G47R mutation of the beta-subunit for ClC-Ka and ClC-Kb chloride channels, barttin, J. Clin. Endocrinol. Metab. 88 (2003) 781–786.

[16] V. García-Nieto, C. Flores, M. Luis-Yanes, E. Gallego, J. Villar, F. Claverie-Martín, Mutation G47R in the BSND gene causes Bartter syndrome with deafness in two Spanish families, Pediatr. Nephrol. 21 (2006) 643–648.

[17] S. Riazuddin, S. Anwar, M. Fischer, Z. Ahmed, S. Khan, A. Janssen, A. Zafar, U. Scholl, T. Husnain, I. Belyantseva, P. Friedman, T. Friedman, C. Fahlke, Molecular basis of DFNB73: mutations of BSND can cause nonsyndromic deafness or Bartter syndrome, Am. J. Hum. Genet. 85 (2009) 273–280.

[18] S. Kitanaka, U. Sato, K. Maruyama, T. Igarashi, A compound heterozygous mutation in the BSND gene detected in Bartter syndrome type IV, Pediatr. Nephrol. 21 (2006) 190–193.

[19] M. Zaffanello, A. Taranta, A. Palma, A. Bettinelli, G. Marseglia, F. Emma, Type IV Bartter syndrome: report of two new cases, Pediatr. Nephrol. 21 (2006) 766–770.

[20] S. Brum, J. Rueff, J. Santos, J. Calado, Unusual adult-onset manifestation of an attenuated Bartter's syndrome type IV renal phenotype caused by a mutation in BSND, Nephrol. Dial. Transplant. 22 (2007) 288–289.

[21] S. Waldegger, N. Jeck, P. Barth, M. Peters, H. Vitzthum, K. Wolf, A. Kurtz, M. Konrad, H. Seyberth, Barttin increases surface expression and changes current properties of ClC-K channels, Pflugers Arch. 444 (2002) 411–418.

[22] A. Hayama, T. Rai, S. Sasaki, S. Uchida, Molecular mechanisms of Bartter syndrome caused by mutations in the BSND gene, Histochem. Cell Biol. 119 (2003) 485–493.

[23] H. Fischer, N. Fukuda, P. Barbry, B. Illek, C. Sartori, M. Matthay, Partial restoration of defective chloride conductance in DeltaF508 CF mice by trimethylamine oxide, Am. J. Physiol. Lung Cell. Mol. Physiol. 281 (2001) L52–L57.

[24] S. Sato, C.L. Ward, M.E. Krouse, J.J. Wine, R.R. Kopito, Glycerol reverses the misfolding phenotype of the most common cystic fibrosis mutation, J. Biol. Chem. 271 (1996) 635–638.

[25] M. Egan, M. Pearson, S. Weiner, V. Rajendran, D. Rubin, J. Glöckner-Pagel, S. Canny, K. Du, G. Lukacs, M. Caplan, Curcumin, a major constituent of turmeric, corrects cystic fibrosis defects, Science 304 (2004) 600–602.

[26] C. Brown, L. Hong-Brown, J. Biwersi, A. Verkman, W. Welch, Chemical chaperones correct the mutant phenotype of the delta F508 cystic fibrosis transmembrane conductance regulator protein, Cell Stress Chaperones 1 (1996) 117–125.

[27] B.K. Tamarappoo, A.S. Verkman, Defective aquaporin-2 trafficking in nephrogenic diabetes insipidus and correction by chemical chaperones, J. Clin. Invest. 101 (1998) 2257–2267.

[28] B. Yang, D. Zhao, A. Verkman, Hsp90 inhibitor partially corrects nephrogenic diabetes insipidus in a conditional knock-in mouse model of aquaporin-2 mutation, FASEB J. 23 (2009) 503–512.

[29] J.P. Morello, A. Salahpour, A. Laperrière, V. Bernier, M.F. Arthus, M. Lonergan, U. Petäjä-Repo, S. Angers, D. Morin, D.G. Bichet, M. Bouvier, Pharmacological chaperones rescue cell-surface expression and function of misfolded V2 vasopressin receptor mutants, J. Clin. Invest. 105 (2000) 887–895.

[30] V. Bernier, J.P. Morello, A. Zarruk, N. Debrand, A. Salahpour, M. Lonergan, M.F. Arthus, A. Laperrière, R. Brouard, M. Bouvier, D.G. Bichet, Pharmacologic chaperones as a potential treatment for X-linked nephrogenic diabetes insipidus, J. Am. Soc. Nephrol. 17 (2006) 232–243.

[31] T. Ohashi, K. Uchida, S. Uchida, S. Sasaki, H. Nihei, Intracellular mislocalization of mutant podocin and correction by chemical chaperones, Histochem. Cell Biol. 119 (2003) 257–264.

[32] L. Ma, Y. Liu, T.M. El-Achkar, X.R. Wu, Molecular and cellular effects of Tamm–Horsfall protein mutations and their rescue by chemical chaperones, J. Biol. Chem. 287 (2012) 1290–1305.

[33] K. Lee, T.J. Hong, J.S. Hahn, Roles of 17-AAG-induced molecular chaperones and Rma1 E3 ubiquitin ligase in folding and degradation of pendrin, FEBS Lett. 586 (2012) 2535–2541.

[34] N. Yui, R. Okutsu, E. Sohara, T. Rai, A. Ohta, Y. Noda, S. Sasaki, S. Uchida, FAPP2 is required for aquaporin-2 apical sorting at trans-Golgi network in polarized MDCK cells, Am. J. Physiol. Cell Physiol. 297 (2009) C1389–C1396.

[35] K. Kamiya, Y. Fujinami, N. Hoya, Y. Okamoto, H. Kouike, R. Komatsuzaki, R. Kusano, S. Nakagawa, H. Satoh, M. Fujii, T. Matsunaga, Mesenchymal stem cell transplantation accelerates hearing recovery through the repair of injured cochlear fibrocytes, Am. J. Pathol. 171 (2007) 214–226.

[36] A. Vandewalle, F. Cluzeaud, M. Bens, S. Kieferle, K. Steinmeyer, T. Jentsch, Localization and induction by dehydration of ClC-K chloride channels in the rat kidney, Am. J. Physiol. 272 (1997) F678–F688.

[37] A. Janssen, U. Scholl, C. Domeyer, D. Nothmann, A. Leinenweber, C. Fahlke, Disease-causing dysfunctions of barttin in Bartter syndrome type IV, J. Am. Soc. Nephrol. 20 (2009) 145–153.

[38] S. Sharp, P. Workman, Inhibitors of the Hsp90 molecular chaperone: current status, Adv. Cancer Res. 95 (2006) 323–348.

[39] L. Pearl, C. Prodromou, P. Workman, The Hsp90 molecular chaperone: an open and shut case for treatment, Biochem. J. 410 (2008) 439–453.

[40] M.A. Dimopoulos, C.S. Mitsiades, K.C. Anderson, P.G. Richardson, Tanespimycin as antitumor therapy, Clin. Lymphoma Myeloma Leuk. 11 (2011) 17–22.

[41] U. Banerji, A. O'Donnell, M. Scurr, S. Pacey, S. Stapleton, Y. Asad, L. Simmons, A. Maloney, F. Raynaud, M. Campbell, M. Walton, S. Lakhani, S. Kaye, P. Workman, I. Judson, Phase I pharmacokinetic and pharmacodynamic study of 17-allylamino, 17-demethoxygeldanamycin in patients with advanced malignancies, J. Clin. Oncol. 23 (2005) 4152–4161.

Hereditary nephrogenic diabetes insipidus in Japanese patients: analysis of 78 families and report of 22 new mutations in AVPR2 and AQP2

Sei Sasaki · Motoko Chiga · Eriko Kikuchi ·
Tatemitsu Rai · Shinichi Uchida

Abstract

Background Familial form of nephrogenic diabetes insipidus (NDI) is a rare hereditary disease caused by arginine vasopressin type 2 receptor (AVPR2) or water channel aquaporin 2 (AQP2) gene mutations. It is speculated that 90 % of NDI families carry disease-causing mutations in AVPR2 and 10 % carry the mutations in AQP2; however, these percentages have not been supported by actual data. It is also unknown whether these percentages vary in different ethnic groups.

Methods Gene mutation analyses were performed for 78 Japanese NDI families. All exons and intron–exon boundaries of the AVPR2 and AQP2 genes were directly sequenced.

Results A total of 62 families (79 %) carried disease-causing mutations in AVPR2, while nine families (12 %) carried mutations in AQP2. We identified 22 novel putatively disease-causing mutations (19 in AVPR2 and 3 in AQP2). Regarding AVPR2, 52 disease-causing mutations were identified. Among them, missense mutations were most common (54 %), followed by deletion mutations. In the 64 women who had monoallelic disease-causing AVPR2 mutations, 16 (25 %) had NDI symptoms, including 4 complete NDI subjects. Regarding AQP2, 9 disease-causing mutations were identified in nine families. Two missense mutations and one deletion mutation showed a recessive inheritance, while one missense mutation and five small deletion mutations in the C-terminus of AQP2 showed a dominant inheritance.

Conclusions Most Japanese NDI families carry disease-causing mutations in AVPR2 and 12 % carry mutations in AQP2. A total of 22 novel putatively disease-causing mutations were identified. The relatively high occurrence of symptomatic carriers of AVPR2 mutations needs attention.

Keywords Aquaporin 2 · Urine concentration · Vasopressin · Vasopressin receptor · Kidney collecting duct

Introduction

Nephrogenic diabetes insipidus (NDI) is a human kidney disease in which the urine-concentrating ability of the kidney cannot respond to the antidiuretic hormone, arginine vasopressin, resulting in the massive excretion of diluted urine. Therefore, NDI patients manifest polyuria and polydipsia. The hereditary (congenital) form of NDI is relatively rare, and is known to be caused by mutations in two genes, the arginine vasopressin type 2 receptor (AVPR2) and the water channel aquaporin 2 (AQP2) [1–4]. These two genes encode two membrane proteins that are oppositely located at the basolateral and apical membranes of the collecting duct principal cells, respectively, and constitute the fundamental components of urine concentrating machinery [5, 6].

The AVPR2 gene is located ion X chromosome (Xq28), and thus, NDI caused by AVPR2 gene mutations is transmitted in an X-linked recessive mode (OMIM 304800); males with one mutated gene are symptomatic, whereas heterozygous females are usually asymptomatic. The AQP2 gene is located on chromosome 12 (12q13.12), and NDI caused by AQP2 mutations shows both autosomal

S. Sasaki (✉) · M. Chiga · E. Kikuchi · T. Rai · S. Uchida
Department of Nephrology, Graduate School of Medical
and Dental Sciences, Tokyo Medical and Dental University,
1-5-45 Yushima, Bunkyo-ku, Tokyo 113-8519, Japan
e-mail: ssasaki.kid@tmd.ac.jp

recessive and dominant inheritance (OMIM 125800, 107777) [7, 8]. Several review papers have claimed that about 90 % of NDI patients carry AVPR2 mutations and about 10 % carry AQP2 mutations; however, actual data in support of this estimate have not been shown [1, 3]. It is also unknown whether the genetic causes of NDI vary among different ethnic groups.

After the cloning of human AQP2 [9] and the first report of an NDI patient with mutated AQP2 [10], we have performed gene mutation analyses of Japanese NDI patients. At the end of July 2012, the total number of analyzed NDI families was 78, a significant number which may provide some insights into the genetic causes of hereditary NDI.

Materials and methods

All NDI families included in this study were referred to our department or visited our outpatient clinic for analysis of gene mutations. Diagnosis of NDI was made in individual facilities based on family histories, clinical symptoms (polyuria and polydipsia, fever due to dehydration), laboratory data (urine and serum osmolalities, serum sodium, serum vasopressin), and responses to water deprivation and/or vasopressin administration. Subjects who presented a milder form of NDI (partial NDI), such as having weaker responses to water deprivation and/or vasopressin administration, were included in this study. Written informed consent for gene mutation analysis was obtained in individual facility. Mutation analyses were performed in our laboratory for most families. Some earlier cases were analyzed in Daniel Bichet's laboratory in Montreal and reported previously [11]. Also, several cases have been reported separately before [12–16]. The AVPR2 and AQP2 genes are relatively small and all exons and intron–exon boundaries were sequenced with usual sequencing methods [12, 17, 18]. Usually, mutation analysis of AVPR2 was performed first. If no causative mutations were found, then AQP2 was analyzed.

Results and discussion

Causative genes in Japanese NDI families

A total of 78 families were referred to us and gene mutation analyses were performed for the AVPR2 and AQP2 genes (Table 1). Gene mutations that presumably cause NDI were identified in the AVPR2 gene in 62 families (79 %), and in the AQP2 gene in nine families (12 %). In the remaining seven families, no mutations were detected in either the AVPR2 or AQP2 genes (Table 1). Of these 78 families, 62 families were newly examined and reported in

Table 1 Causative genes in Japanese Nephrogenic diabetes insipidus (NDI) families

Causative genes	Number of families
AVPR2	62 (79 %)
New in this report	49
Previously reported	13
AQP2	9 (12 %)
New in this study	6
Previously reported	3
Not found	7 (9 %)
Total	78

this paper. A total of 22 novel putatively disease-causing mutations that have not been previously reported or included in the public database (HGMD: http://www.hgmd.cf.ac.uk/ac/index.php) were identified in this study (19 in AVPR2 and 3 in AQP2).

If the seven families with no mutations are excluded, AVPR2 accounts for 87 % of gene defect-identified cases, while AQP2 accounts for 13 %. These data provide clear evidence for the general assumption that 90 % of cases are caused by AVPR2 and 10 % are caused by AQP2 mutations [1, 3]. These data also indicate that the genetic mechanisms for congenital NDI are the same in the Japanese population.

More than 220 disease-causing mutations have been reported for AVPR2 [19], and 50 disease-causing mutations have been reported for AQP2 [7, 20]. Our present report of 22 new putatively disease-causing mutations significantly increases the numbers of known NDI-causing mutations by about 10 %. When new mutations are found, it must be determined if they are disease causative or not. This determination is usually done by examining associations between the genotype and phenotype within the family (a comparison of subjects harboring the mutation and expression of clinical symptoms) and by examining functions of the mutated gene product in heterologous expression systems. In the present study, the functions of the mutant proteins were not examined, which is a limitation of the present study.

Disease-causing AVPR2 mutations in 62 NDI families

A total of 52 putative disease-causing AVPR2 mutations were identified in 62 families (several mutations were shared by different independent families). Table 2 summarizes the types of AVPR2 mutations. Gene variants/polymorphisms that have been reported not to cause NDI [19] were excluded in this summary. Missense mutations were most common, accounting for half of the mutations, followed by deletion mutations, insertion mutations, and

nonsense mutations. Splicing mutations were the least common. This relative frequency of disease-causing AVPR2 mutations is consistent with the results of a worldwide summary of AVPR2 mutations, as shown in Table 2 [19], again confirming that the genetic mechanisms causing NDI are the same in different ethnic groups [19].

Of these AVPR2 mutations, 19 mutations were novel, and the other mutations were previously reported or recurrences of the previously reported mutations. Details of the novel AVPR2 mutations are summarized in Table 3. In brief, in a family carrying the missense mutation D85E, an index subject was a female patient manifesting complete NDI, and her father also manifested NDI. The index subject was heterozygous for this mutation. The codon Asp85 seems functionally important, because another missense mutation on this residue, D85N, was reportedly causative in six families [19]. L90P was observed in two unrelated families. In one family, the index case was a mother of a boy with NDI; they manifested partial and complete NDI, respectively, and the mother was a heterozygous carrier of the mutation. In another family, a boy showed complete NDI, and his mother was a heterozygous carrier of the mutation with no NDI symptoms. K116N mutation was found in a boy with complete NDI, and his mother was not a carrier of the mutation, implying that the mutation occurred de novo. M123R mutation was observed in two unrelated families in which the index patients were boys with complete NDI. DNA samples of other members of the families were not available, and a mother in one family had polyuria and polydipsia. M123R has not been previously reported, but another mutation on this residue, M123K, has been reported [11]. L131P were found in two young brothers with complete NDI, and their mother was a heterozygous carrier of the mutation with no NDI symptoms. Mutation on Leu131 has not been reported, but missense mutations on encompassing residues, I130L, I130F and A132D have been shown to be causative [19], indicating that this region is functionally important. W164R was found in a boy with NDI, and his mother was a heterozygous carrier of the mutation. On Trp164, another mutation, W164S, has been reported [17], and mutations on Ala165 and Ser167 were also shown to be causative [19]. Q225R was found in a boy with complete NDI, and his mother was a heterozygous carrier without symptoms, while his healthy brother was not affected. L316R was found in a boy with complete NDI, and his mother was a heterozygous carrier. Leu316 has not been the target of missense mutations, while encompassing residues Ser315 and Asn317 located in the 7th transmembrane domain of AVPR2 protein are the target of disease-causing mutations, S315R and N317K [19]. S329G was found in a boy with complete NDI. His mother and grandmother were asymptomatic heterozygous carriers of the mutation, and his uncle had the same

Table 2 Types of AVPR2 mutations in Japanese Nephrogenic diabetes insipidus (NDI) patients and comparison with a global summary

Types of mutations	Number of mutations identified in Japanese patients[a]	Relative frequency in a global summary[b] (%)
Missense	28 (54 %)	56
Nonsense	4 (8 %)	13
Deletion	13 (25 %)	29
Insertion	5 (10 %)	4
Splicing	2 (4 %)	1

[a] A total 52 mutations were identified in this study

[b] Relative frequency reported by Spanakis et al. [19]

Table 3 New putative disease-causing AVPR2 mutation

	Nucleotide change	Amino acid change
Missense	c.255C>A	D85E
	c.269T>C	L90P
	c.348G>C	K116N
	c.368T>G	M123R
	c.392T>C	L131P
	c.490T>C	W164R
	c.674A>G	Q225R
	c.947T>G	L316R
	c.985A>G	S329G
	c.985_986AG>CC	S329P
Nonsense	c.624G>A	W208X
Deletion	c.91_92 del AC	FS/190X
	c.521delA	FS/211X
	c.1055_1068delGTCCCCAAGATGAG	FS/376X
	5′UTR-AVPR2_DEL 4,586	Large del of AVPR2
	5′UTR-AVPR2_DEL 32,787	Large del of AVPR2
Insertion	c.369_370insT	FS/191X
	c.498_499insTC	FS/212X
	c.738_739insG	FS/257X

mutation with complete NDI symptoms. S329P was found in a boy with complete NDI, and his mother was an asymptomatic heterozygous carrier. Another mutation on Ser329, S329R, has been reported [21].

A nonsense mutation, W208X, was observed in a boy with complete NDI, and his asymptomatic mother and sister were heterozygous carriers of the mutation. To date, all reported nonsense mutations have been shown causative [19].

Five novel deletion mutations were found, and all these mutations cause either large losses of the gene, including the 5′ untranslated region (two families), or frame shifts that result in premature truncation (two families) or